Applied Thermal Engineering 258 (2025) 124630

Contents lists available at ScienceDirect

Applied Thermal Engineering

journal homepage: www.elsevier.com/locate/apthermeng

Research Paper

Experimental investigation into heat transfer and flow characteristics of magnetic hybrid nanofluid (Fe_3O_4/TiO_2) in turbulent region

Victor O. Adogbeji [a], Mohsen Sharifpur [a,b,c,*], Josua P. Meyer [a,d]

[a] Department of Mechanical and Aeronautical Engineering, University of Pretoria, Pretoria, Private Bag X20, Hatfield 0028, South Africa
[b] School of Mechanical, Industrial and Aeronautical Engineering, University of the Witwatersrand, Private Bag 3, Wits 2050, South Africa
[c] Department of Medical Research, China Medical University Hospital, China Medical University, Taichung, Taiwan
[d] Department of Mechanical and Mechatronic Engineering, Stellenbosch University, Stellenbosch, South Africa

ARTICLE INFO

Keywords:
Fe_3O_4/TiO_2 nanofluids
Force convective heat transfer
Hydraulic resistance
Pressure drop
Heat transfer enhancement

ABSTRACT

Extensive research and empirical evidence demonstrate the superior thermal performance of nanofluids compared to DIW. Magnetic hybrid nanofluids, such as Fe_3O_4/TiO_2, are currently being explored for their enhanced thermal properties. This study evaluates Fe_3O_4/TiO_2 nanofluids for heat transfer and hydraulic resistance across Reynolds numbers from 3200 to 5300 and volume fractions from 0.00625 % to 0.3 % vol. UV–Vis spectroscopy shows that lower volumetric fractions correlate with decreased sedimentation. Over 30 days, nanofluids with 0.3 % vol, 0.2 % vol, and 0.1 % vol exhibited high sedimentation factors (SF) of 31.79 %, 11.88 %, and 11.44 %, respectively, while 0.00625 % vol, 0.0125 % vol, and 0.025 % vol demonstrated better stability with SFs of 8.89 %, 9.82 %, and 10.24 % respectively. Volume fractions significantly impact heat transfer, with CHT coefficients increasing by 11.42 % at 0.3 % vol, 14.03 % at 0.2 % vol, 18.04 % at 0.1 % vol, and 19.98 % at 0.05 % vol. The greatest enhancements are at lower concentrations: 22.91 % at 0.025 % vol, a peak of 26.33 % at 0.0125 % vol, and 24.30 % at 0.00625 % vol. Pressure drops are highest at 21 % for 0.3 % vol at Re 5018, decreasing with lower concentrations: 13.10 % at Re 5144.4 (0.2 % vol), 11.94 % at Re 5041.6 (0.1 % vol), 9.82 % at Re 5112.2 (0.05 % vol), 7.67 % at Re 5258.7 (0.0125 % vol), and 10.29 % at Re 5094.0 (0.00625 % vol). These results highlight that higher nanoparticle concentrations increase pressure drop, impacting energy efficiency. Lower concentrations (0.0125 % Vol and 0.00625 % Vol) provided better heat transfer with lower pressure losses. Total Efficiency Index (TEI), The optimal nanoparticle concentration for maximum thermal efficiency was approximately 0.0125 % Vol. TEI values were highest at this concentration, indicating enhanced heat transfer with minimal thermal resistance and pressure drop. Higher concentrations (0.2 % Vol and 0.3 % Vol) showed lower TEI values, suggesting reduced thermal efficiency due to increased flow resistance. These findings highlight the importance of selecting an appropriate nanoparticle concentration to optimize thermal performance in heat transfer systems, balancing the benefits of enhanced heat transfer with the drawbacks of higher-pressure losses.

1. Introduction

Enhancing heat transfer efficiency remains a prominent challenge in various applications involving heat exchangers and heat transfer processes. Extensive research has been undertaken to advance convective exchange transfer capabilities by leveraging advanced nanotechnology. Nanofluids (NFs) have shown enhanced heat transfer attributes when contrasted with conventional working fluids like oil, ethylene glycol (EG), and water. This improvement arises from incorporating nanoparticles with exceptional thermal transport characteristics into NFs, enhancing their overall thermal characteristics. NFs are created by dissipating these nanoscale particles within a base fluid. It's important to note that at the nanoscale level, interatomic forces play a significant role and must be considered when characterizing experiments and modelling the behaviours of nanomaterials. Notably, the concept of NFs was first explored by Choi and Eastman in 1995, marking a pivotal moment in research [1]. Since then, numerous scientists have investigated the impact of various nanoparticles, such as Fe_3O_4, SiO_2, CNT, MCNT, CuO, Al_2O_3, and TiO_2, on enhancing CHT through alterations in thermal properties and fluid behavior [2]. Ahmed and Eslamian [3] have studied the impact of external forces such as gravitational,

* Corresponding author at: Department of Mechanical and Aeronautical Engineering, University of Pretoria, Pretoria, Private Bag X20, Hatfield 0028, South Africa.
E-mail address: mohsen.sharifpur@up.ac.za (M. Sharifpur).

https://doi.org/10.1016/j.applthermaleng.2024.124630
Received 20 May 2024; Received in revised form 4 October 2024; Accepted 10 October 2024
Available online 12 October 2024

Abbreviations

Al	Aluminium nanoparticles
AL_2O_3	Aluminium oxide nanoparticles
Au	Gold nanoparticles
Co_2O_3	Cobalt (III) oxide nanoparticles
Cu	Copper nanoparticles
CuO	Copper oxide nanoparticles
CHT	Convective heat transfer
CNTs	Carbon nanotubes
DC	Direct current
Di	Internal diameter of the tube
DIW	Deionised water
DW	Distilled water
EG	Ethylene glycol
Fe_2O_3	Iron (III) oxide nanoparticles
Fe_3O_4	Iron (IV) oxide nanoparticles
G	Gauss
GA	Gum Arabic
GMO	Graphene magnetite oxide
I	Current (Ampere)
MF	Magnetic fields
MHNFs	Magnetic hybrid nanofluids
MNFs	Magnetic nanofluids
MNPs	Magnetic nanoparticles
MWCNT	Multiwalled carbon nanoparticle
mT	Millitesla
Nu	Nusselt number
Pr	Prandtl number
Re	Reynolds number
SF	Sedimentation Factor
SiO_2	Silicon oxide nanoparticles
STDEV	Standard deviation
TEM	Transmission electron microscopy
TiO_2	Titanium oxide nanoparticles
TEI	Total efficiency index
UV-Vis	Ultra Violet-Visible
V	Voltage
x/d	Axial distance

Greek symbols

φ	Mass ratio of nanofluids
Φ	Volume concentration (vol%)
μ	Viscosity (kg/m.s)
K	Thermal conductivity (W/K^{-1})
σ	Electrical conductivity (mS/cm^{-1})
ρ	Density (Kg/m^3)
η	Thermal efficiency
$\dot{q}$	Heat flux, (W/m^2)
$\dot{m}$	Mass flow rate (Kg/s)

Subscripts

A_o	Initial Absorbance
A_t	Final Absorbance
avg	Average
u_B	Bias error
u_p	Precision error
bf	base fluid
C_p	Specific heat capacity of particles (J/kg-K)
C_{pnf}	specific heat capacity of nanofluids (J/kg-K)
C_{pbf}	specific heat capacity of base fluids (J/kg-K)
C_{pnp}	specific heat capacity of nanoparticles (J/kg-K)
ρ_{nf}	Densities of the nanofluid (Kg/m^3)
ρ_{bf}	Density of base fluid (Kg/m^3)
$\varphi\rho_{np}$	Density of nanoparticles (Kg/m^3)
h_{avg}	Average heat transfer coefficient (W/m^2-K)
t_O	outlet °C
t_i	inlet °C
t_w	wall temperature °C
t_b	bulk temperature °C
n_f	nanofluid
n_p	nanoparticles

thermophoretic, and Brownian forces on particle dynamics in nanofluids and aerosol systems, highlighting their role in influencing nanoparticle stability and heat transfer performance. Similarly, Nasir et al. [4] enhanced the thermal performance of convective flow using a water-based trihybrid nanofluid across a Riga plate, incorporating nanocomposites of carbon nanotubes in spherical form, graphene in cylindrical form, and Al_2O_3 in platelet form.

Researchers are increasingly exploring the category of unique nanofluids (NFs) by incorporating magnetic particles like nickel, iron, and cobalt into standard working fluids [5,6]. Ferrofluids consist of nanoscale magnetic particles dispersed in a carrier liquid, often an organic solvent or water, with iron oxides like Fe_2O_3 (hematite) and Fe_3O_4 (magnetite) being common choices. Among these, Fe_3O_4 stand out due to its exceptional response to magnetic fields, making it intriguing for various applications [7]. Fe_3O_4 stand out due to their capacity to modify physical properties in a controlled manner when subjected to an external magnetic field is utilized in various applications. When influenced by a magnetic field, the optical, thermal, and rheological characteristics of ferrofluids can be finely adjusted, classifying them as 'intelligent' fluids. [8]. This exceptional performance underscores its potential for various applications.

However, research conducted by Karamallat et al. [9], Sha et al. [10], Ajeena et al. [11], and Yildiz [12] closely analysed convective heat transfer using densely packed oxide nanoparticles and their outcomes led to higher viscosity in the nanofluid, thereby increasing the energy needed for pumping. For instance, Fu et al. [13] investigated the turbulent heat transfer properties of Fe_3O_4 nanofluids in a circular pipe, where the nanofluids were composed of a mixture of Fe_3O_4/EG/DIW. The Fe_3O_4 nanoparticles were treated with citric acid to enhance their dispersion. The study assessed the performance of these nanofluids over a range of volume fractions from 0.0 wt% to 1.2 wt%. They found that achieving effective CHT necessitated significant adjustments in heat flux, fluid flow rate, and temperature. Additionally, it was observed that the CHT coefficient of the nanofluid was 7 % lower compared to the base liquid. Sundar et al. [14] examined Fe_3O_4 magnetic nanofluids in vacuum pump oil under laminar flow, noting a 9 % improvement in thermal conductivity at a 0.5 % volume concentration. However, this improvement was accompanied by 1.75 times increase in viscosity and a higher friction factor. CHT rose by 13.1 % and 17.8 %, and the Nusselt number increased by 8.95 % and 13.48 % for mass flow rates of 0.0416 kg/s and 0.208 kg/s. However, this improvement led to a 1.21 times higher friction factor when evaluated alongside the base liquid. In contrast, Sundar et al. [15] conducted an experimental evaluation of the CHT coefficient and friction factor of Fe_3O_4 nanofluids in a circular tube, examining Re from 3000 to 22,000 and volumetric fractions ranging from 0 % to 0.6 %. They found that the heat transfer performance of the nanofluids exceeded that of water and improved with increasing volume concentration. Specifically, they reported a 30.96 % increase in heat transfer and a 10.01 % rise in friction factor for Fe_3O_4 nanofluids at a 0.6 % volume fraction under turbulent flow conditions. Askari et al. [16]

they examined the convective heat transfer of Fe_3O_4/graphene nanofluids in a turbulent flow within a straight tube at Reynolds numbers of 2000–5000 and volumetric fraction of 0.1 %, 02–1 %. They observed a 14–32 % increase in thermal conductivity for 1 % volume fraction of Fe_3O_4 and Fe_3O_4/graphene nanofluids at 20 °C and 40 °C when evaluated alongside the base liquid. Additionally, they noted an 8.5 % enhancement in the convective heat transfer coefficient for Fe_3O_4 nanofluids and a 14.5 % increase for Fe_3O_4/graphene nanofluids. Alsarraf et al. [17] investigated Fe_3O_4/CNT hybrid nanofluids and observed notable enhancements in the average Nu compared to water. For nanofluids with 0.5 % ferrofluid, 0.7 % ferrofluid, and 0.9 % ferrofluid concentrations, the Nu increased by 17.25–18.7 %, 20.17–27.25 %, and 23.18–38.83 % respectively, in the Re range of 500–2000. At 0.5 % ferrofluid with 0.25 % CNT and 0.9 % ferrofluid with 1.35 % CNT, Nu improvements were 17.45–19.57 % and 23.51–52.54 % respectively. Conversely, the pressure drop for these nanofluids was significantly higher compared to water, with increases of 31.28–38.1 %, 106.82–110.88 %, and 185.16–190.48 % for 0.5 % ferrofluid, 0.7 % ferrofluid, and 0.9 % ferrofluid concentrations, respectively. For 0.5 % ferrofluid with 0.25 % CNT and 0.9 % ferrofluid with 1.35 % CNT, the pressure drop rose by 73.96–78.78 % and 314.49–321.77 %, respectively. The higher concentration of nanoparticles led to increased flow velocity and a thinner velocity boundary layer, resulting in greater pressure drop. Asfer et al. [18] experimental investigations on water-based ferrofluid in a heated tube influenced by permanent magnets revealed that heat exchange improvement relies on the magnetic force's magnitude relative to inertia force, interconnected structures among nanoparticles, and ferrofluid-nanoparticle interaction near the tube wall. Sundar et al. Sundar et al. [19] experimentally assessed the thermal–hydraulic properties of a Fe_3O_4/CNT/water hybrid nanofluid flowing through a tube. Their study revealed a 14.81 % increase in the Nu at a 0.3 % nanoparticle concentration when the Re was 3000. Yarahmadi et al. [20] conducted experimental evaluations of Fe_3O_4/water nanofluids with volume fractions ranging from 1.5 wt% to 5 wt% at Reynolds numbers from 100 to 500. They found that the highest improvement in the local convective heat transfer coefficient occurred at the end of the magnetic field application along the flow path of the ferrofluid. Specifically, at a Re of 465 and a 5 % volume fraction with a magnetic field frequency of 50 Hz, the heat transfer enhancement reached 19.8 % compared to the scenario without a magnetic field. Abadeh et al. [21] carried out experiments utilizing a ferrofluid containing Fe_3O_4 nanoparticles in water to investigate in a circular straight tube in the laminar regime, The outcome revealed enhanced heat transfer coefficients, Nu when evaluated alongside to pure water across various Re. Significant Nu improvement occurred under constant magnetic fields (1300 and 770 G) with four types of patterns. Additionally, Nu increased by 11.85 % and 14.8 % with alternating magnetic fields at 10 Hz and 100 Hz but showed no significant improvement beyond 100 Hz. Sun et al. [22] in an experiment with hydromagnetic nanofluids containing Fe_3O_4 nanoparticles, the impact of magnetic fields on CHT was evaluated. Higher magnetic flux density (415 gauss) notably improved heat transfer by 4.36 % at a Re of 1080, and a 700-gauss field enhanced it by 7.19 %. A field gradient of 28.6 gauss/mm induced chain-like structures, resulting in a significant 32.0 % local Nusselt number increase. Despite increasing pressure drop due to flow disturbance, the heat transfer enhancement prevailed. The study covered Reynolds numbers from 400 to 2000 and volumetric fraction of Fe_3O_4 nanoparticles from 0.1 % to 0.9 %. Goharkhah et al. [23] carried out experimental investigations on Fe_3O_4 nanofluids in water, reporting a 13.5 % enhancement in convective heat transfer with Fe_3O_4 nanofluids. The study measured local CHT coefficients in both thermally developing and fully developed regions for volume fractions of 1 %, 1.5 %, and 2 %, within the Re range of 400–1200. The researchers also simulated magnetic fields and force distributions to better understand the improvements in heat transfer. Without a magnetic field, Fe_3O_4 nanofluid at a 2 % volume fraction increased average CHT by 13.5 % compared to deionized water at Re 1200. When a constant magnetic field with an intensity of 500 G was applied, this improvement rose to 18.9 %, and it reached 31.4 % with an alternating magnetic field. Tekir et al. [24] conducted experiments with Fe_3O_4 nanofluids under laminar flow ($1122 < Re < 2124$) and applied a constant heat flux to the pipe surface. They examined the impact of parameters such as Re, nanoparticle volume fraction (0–0.05), and both constant and alternating magnetic fields with various waveforms (sine, square, triangle) and frequencies (2, 5, and 15 Hz) on convective heat transfer. Results indicated a 13 % improvement in heat transfer with a constant magnetic field compared to no magnetic field, while alternating magnetic fields boosted convective heat transfer by up to 35 %. Mei et al. [25] conducted a study with a Re of 600–1100 and with nanoparticle mass fractions varying from 1.0 % to 5.0 %, thermohydraulic performance was evaluated in a copper tube using Fe_3O_4 magnetic nanofluids. Nu increased by 10.0 % with magnetic intensity and 17.6 % with nanoparticle mass fraction, with more significant improvements in corrugated tubes. Azizian et al. [26] performed experiments with Fe_3O_4 nanofluids under laminar flow at a 0.86 wt% concentration. They found that increasing the strength and gradient of the magnetic field significantly enhances the local heat transfer coefficient, especially at higher Re. At Re 745, with a magnetic field gradient of 32.5 mT/mm, the heat transfer enhancement was four times greater compared to the scenario without a magnetic field. The impact of the magnetic field on pressure drop was relatively minor, increasing by up to 7.5 % with magnetic field intensities of 430 mT and gradients ranging from 8.6 to 32.5 mT/mm. Wang et al. [27] investigated the performance of Fe_3O_4 nanofluids with volumetric fraction of 1.8 %, 2.6 %, and 5.2 % under laminar flow conditions across Re from 0 to 1000. Their study demonstrated that increasing the magnetic flux density, achieved by adding more magnets, significantly enhances heat transfer. Specifically, with the use of five magnetic cannulas, the heat transfer improvements were 26.5 % at Re 391 and 54.5 % at Re 805. However, this enhancement was accompanied by a high pressure drop. Hatami et al. [28] experiments using Fe_3O_4 nanofluid in water evaluated the impact of a magnetic field on laminar CHT (Reynolds number 100–500, nanoparticle mass fractions 0–1.8 %). Surprisingly, the increase of magnetic nanoparticles increased CHT by over 60 %, even as magnetic fields reduced the convective heat transfer coefficient by 25 %. Furthermore, increasing the Hartmann number for a given nanofluid volumetric fraction led to a 25 % decline in heat exchange rate. Ahangar et al. [29] in a vertical tube experiment with magnetic quadrupole fields showed significant increases in local heat transfer coefficients, up to 48.9 % for 2 vol% Fe_3O_4 magnetic nanofluid at Re 580. This improvement was ascribed to the radial magnetic force directing the ferrofluid towards the heated wall. Ghofrani et al. [30] in experiments with aqueous ferrofluid in copper tube subjected to both a constant heat flux and alternating magnetic field, CHT improved by 27.6 % compared to water. Raising the magnetic field frequency or increasing the volumetric fraction of nanoparticles improved heat exchange, particularly at lower Re. Lajvardi et al. [31] in copper tube experiments with ferrofluid at Re from 0 to 265 and nanoparticle mass fractions of 2.5–5 %, the applied of magnetic fields improve heat exchange by altering the ferrofluid's thermophysical properties. Sha et al. [10]. In turbulent flow experiments with Fe_3O_4 in water Re 4000–6500 and nanoparticle mass fractions 0.5–3 %, perpendicular magnetic fields (uniform and gradient) enhanced heat transfer coefficients. Stronger magnetic fields and higher nanoparticle concentrations led to more significant improvements, with maximum average enhancements of 4.2 % and 8.1 % for constant and gradient magnetic fields, respectively. Guzei et al. [32] in forced convection experiments with magnetic nanofluids at a constant 0.3 T magnetic field, a 35 % improvement in the average heat exchange efficiency was observed when evaluated alongside the base fluid at a fixed Re. without of the magnetic field, a 10 % improvement was noted in pure nanofluids evaluated alongside the pure water. Ebaid et al. [33] study Fe_3O_4/water in heated tube experiments with Re 2180–9160, nanoparticle volume fractions 0.3–1.2 %, the Nu enhanced by 16.7 %

evaluated alongside the water without a magnetic field. Application of magnetic fields (15.5–45.5 mT) led to 9.4–31.3 % enhancements in the average heat exchange efficiency and Nu. The majority of experimental research has predominantly centered on single nanofluids, particularly Fe_3O_4, often using densely packed oxide nanoparticles. This approach can lead to increased viscosity and higher energy requirements for pumping. While studies on CHT have extensively explored hybrid nanofluids, especially combinations like Fe_3O_4/graphene, MWCNT/Fe_3O_4 and CTNs/Fe_3O_4, most of this work has been conducted under laminar flow conditions. There remains a significant gap in the literature concerning hybrid combinations and turbulent flow regimes, particularly involving Fe_3O_4 mixed with other nanomaterials. Existing research predominantly concentrates on high-volume nanoparticle concentrations, often emphasizing the impact of these concentrations on heat transfer. However, these studies frequently report a disproportionately low percentage of heat transfer enhancement relative to the significant increase in pumping requirements. This imbalance underscores the need for further investigation into optimizing nanoparticle concentrations to achieve a more efficient trade-off between enhanced thermal performance and energy consumption. The choice of Fe_3O_4 and TiO_2 nanoparticles for this research is grounded in their distinct yet complementary properties, which are crucial for investigating MHNFs. Fe_3O_4, or magnetite, was selected for its strong magnetic characteristics, essential for manipulating the nanofluid using external magnetic fields. This manipulation is critical for enhancing heat transfer in various applications, as magnetic fields can influence both fluid flow and thermal conductivity. TiO_2, on the other hand, was chosen for its excellent thermal conductivity, chemical stability, and relatively high specific surface area, all of which significantly contribute to improved heat transfer efficiency and overall stability of the nanofluid. Additionally, TiO_2's photocatalytic properties offer potential advantages in specific applications beyond heat transfer. By combining Fe_3O_4 and TiO_2, this research seeks to explore the synergistic effects of magnetic and thermal properties, providing valuable insights into their impact on the thermophysical properties of nanofluids. This study aims to investigate new combinations and their potential advantages in thermal applications, distinguishing itself from regularly used hybrid nanofluids, such as Fe_3O_4/graphene, MWCNT/Fe_3O_4 and CNTs/Fe_3O_4 hybrids. Existing research consistently shows that MHNFs exhibit more significant enhancements in CHT compared to single nanofluids. However, the extent of these improvements in MHNFs is not sufficiently represented in the literature. Furthermore, there is a limited experimental examination of CHT enhancements in MHNFs that combine Fe_3O_4 with other nanoparticles. This study aims to determine the optimal nanoparticle concentration of Fe_3O_4/TiO_2 nanofluids with an 80:20 ratio under turbulent flow conditions to balance enhanced thermal performance with energy efficiency. The primary objective is to identify the concentration that maximizes convective heat transfer while minimizing the associated pressure drop and energy consumption, particularly in turbulent flow conditions. By doing so, this research seeks to advance the understanding of how magnetic hybrid nanofluids can be optimized for industrial applications, contributing to the state-of-the-art by providing a more energy-efficient solution to heat transfer challenges. The successful achievement of these objectives would not only validate the potential of Fe_3O_4/TiO_2 nanofluids in enhancing thermal systems but also offer practical insights for their implementation in real-world scenarios, where energy efficiency and thermal performance are critical.This study systematically examine CHT and pressure drop characteristics of these hybrid nanofluids across various volumetric fractions (0.00625–0.3 %) using DIW as the base fluid within the turbulent flow range (Re 3200–5400).

2. Experimental set-up and procedure

2.1. Preparation and characterization of MHNFs

The magnetic nanoparticles consisted of iron (III) oxide (Fe_3O_4) with a nano size of 20–30 nm and a purity of 95.5 %. Titanium dioxide (TiO_2) with an 18 nm diameter and a purity of 99.9 % was also used, with the particle size matching the manufacturer's specifications. The Ti O_2 nanoparticles were obtained from Nanostructured and Amorphous Materials Inc. in Houston, Texas, USA, while the rest were purchased from US Research Nanomaterial Inc. in Houston, Texas, USA. To improve the hybrid nanofluids stability, Gum Arabic (GA) with a purity of ≥98.5 % from Sigma-Aldrich in Berlin, Germany, was employed as a surfactant. The thermal properties of both the base fluid and the nanoparticles utilized in the research can be found in Table 1, with certain material characteristics and parameters sourced from the product datasheets provided by the respective companies.

The preparation of magnetic hybrid nanofluids (MHNFs) follows a two-step method. Step 1, Weighing nanoparticles involves combining Fe_3O_4 and TiO_2 nanoparticles at an 80–20 % ratio using a digital balance (Radwag AS 220.R2, Radom, Poland, ±0.01 g accuracy**).** Step 2, adding surfactant incorporates Gum Arabic at a weight ratio of 0.75 to stabilize the nanoparticles. In step 3, Dispersing nanoparticles, the nanoparticles are initially mixed with a mechanical stirrer, then dispersed in DIW using ultrasonication with a Qsonica Q-700 Ultrasonicator for 4 h, employing a sequence of 5-second pulses and 2-second intervals. Step 4, Temperature control maintains a consistent temperature of 20 °C during dispersion with a programmable water bath (LAUDA ECO RE1225). Finally, in Step 5, the resulting nanofluid involves preparing MHNFs with volume concentrations ranging from 0.00625 % to 0.3 %, which are then assessed for stability and thermophysical properties. Fig. 1 provides a visual representation of this process, and Eq. (1) [34] is used for calculating the nanoparticles.

$$\varphi = \left(\frac{Y_{Fe_3O_4}\left(\frac{W}{\rho}\right)_{Fe_3O_4} + Y_{TiO_2}\left(\frac{W}{\rho}\right)_{TiO_2}}{Y_{Fe_3O_4}\left(\frac{W}{\rho}\right)_{Fe_3O_4} + Y_{TiO_2}\left(\frac{W}{\rho}\right)_{TiO_2} + \left(\frac{W}{\rho}\right)_{DIW}} \right) \quad (1)$$

Were Y being the ratio of the nanoparticles.

Various pieces of equipment were employed for diverse purposes in the study. These instruments included a pH meter (Jenway 3510, Staffordshire, UK) with a range of −2 to 19.999 and an accuracy of ±0.003, a vibro-viscometer (SV-10A series, A&D, Tokyo, Japan) with an accuracy of ±1 %, a UV–visible spectrophotometer (Jenway, Staffordshire, UK), a transmission electron microscope (JEOL JEM-2100F, Tokyo, Japan) for examining dry samples, and a conductivity meter (CHAUVIN ARNOUX, C.A 10141 Instrument, France) with an accuracy of ±1 %. These instruments served various roles in the research, enabling thorough analysis and precise measurements. Additionally, the prepared MHNFs underwent characterization for thermal conductivity (κ) and viscosity (μ) across different temperatures, from 10 °C to 50 °C. This

Table 1
Thermal properties of the materials under investigation at standard room temperature.

Properties	Deionized water (DIW)	Iron (III) oxide (20–30 nm)	Titanium dioxide(18 nm)
Density (kg/m^3)	997	4950	4175
Thermal conductivity (W/m.K)	0.613	80.4	8.4
Specific Heat capacity (J/kg.K)	4179	670	692
shape	–	Plate-likenanosheet	spherical

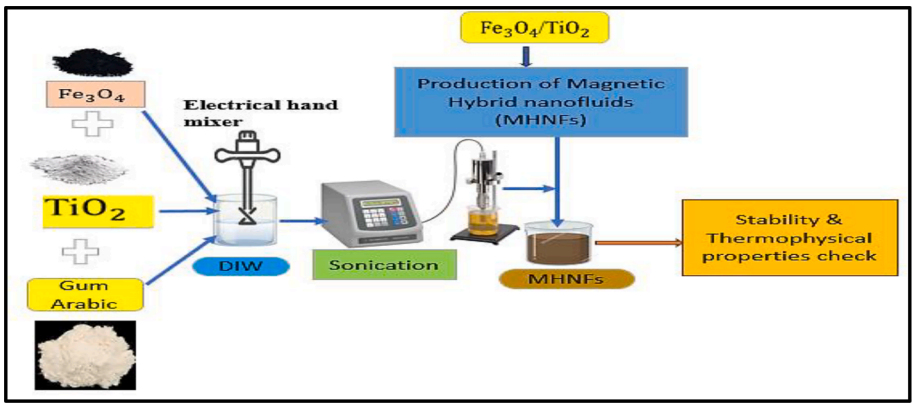

Fig. 1. Schematic of the preparation process for MHNFs.

analysis was done using the KD2 pro (Decagon Devices Inc). This approach enabled the evaluation of the thermal properties of magnetic hybrid nanofluids (MHNFs) under various temperature conditions. We utilized a range of techniques and instruments to ensure precision and reliability in assessing the stability, thermophysical properties, and other characteristics of MHNFs. For instance, transmission electron microscopy (TEM) was employed to analyse the morphology and distribution of the nanofluids. Stability was monitored using multiple methods, including viscosity measurements, UV–visible spectrophotometry, thermal conductivity assessments, and macroscopic observations, as shown in Fig. 2. To confirm the stability of the MHNFs, these properties were examined and kept constant throughout the stability evaluation period. Our study included comprehensive analyses through UV–visible spectrophotometry, thermal conductivity measurements, and viscosity tests, conducted immediately after sonication and after 24 h, across temperatures ranging from 10 °C to 50 °C. Additionally, visual inspections were performed weekly over one month.

2.2. UV–visible spectrophotometry

MHNF were analysed via UV–Vis spectroscopy using an ONDA TOUCH UV-21 Spectrophotometer at room temperature. DIW served as the standard. Each measurement was repeated six times, and averages were calculated. The light spectrum covered wavelengths from 200 to 300 nm, with 10 nm intervals from 200 to 280 nm and 1 nm intervals from 281 to 300 nm for all samples. The absorbance of MHNFs at different wavelengths and sedimentation percentage was determined using Eq. (2).

$$\text{Percentage (SF)} = \left(\frac{\textit{Maximum absorbance} - \textit{Total average absorbance}}{\text{Maximum absorbance}}\right) \times 100 \quad (2)$$

2.3. Setup used for measuring thermal, electrical conductivity and pH

In this study, the experimental setup comprised two main components: the section for measuring thermal conductivity and the constant temperature bath. To maintain precise temperature control, we employed a programmable water bath. Thermal conductivity measurements were conducted continuously for 24 h, covering a temperature range from 10 °C to 50 °C with intervals of 5 °C. MHNFs' thermal conductivity was determined using the KD2 pro instrument manufactured by Decagon Devices Inc. This instrument operates within a specified range of 0.02 $W{\cdot}m^{-1}{\cdot}K^{-1}$ to 2 $W{\cdot}m^{-1}{\cdot}K^{-1}$, with a manufacturer-stated uncertainty level of 5 %. To ensure accurate readings, it is essential to maintain a minimum of 15 mm of the material being measured parallel to the sensor in all directions, as the sensor emits a heat pulse. The electrical conductivity and pH of the fluid were additionally assessed, with temperature variations ranging from 10 °C to 50 °C at 5 °C intervals, as illustrated in Fig. 2b.

2.4. Measurement of viscosity

Viscosity is a crucial thermophysical property used to evaluate the stability of nanofluids. In this research, we conducted viscosity measurements of MHNFs (Fe_3O_4/Ti O_2/DI Water) to assess their stability across a temperature range spanning from 10 °C to 50 °C. Before measuring the viscosity of the nanofluids, we ensured the accuracy of the vibro-viscometer through calibration. To maintain a consistent temperature during the experiment, the vibro-viscometer jacket was connected to a programmable water bath (LAUDA, Berlin, Germany, model ECO RE1225) and a data logger, as shown in Fig. 2a. The MHNFs' temperature was adjusted between 10 °C and 50 °C in 5 °C increments. Initial viscosity measurements were taken immediately after preparing the nanofluids, and we continued to monitor them for 24 h to check the stability of each volume fraction. This allowed us to comprehensively evaluate the viscosity of MHNFs under varying temperatures and over different time intervals.

2.5. Nanoparticle morphology analysis in MHFs

The analysis of nanofluids containing Fe_3O_4 and varying proportions of TiO_2 involved investigating their morphology and stability using

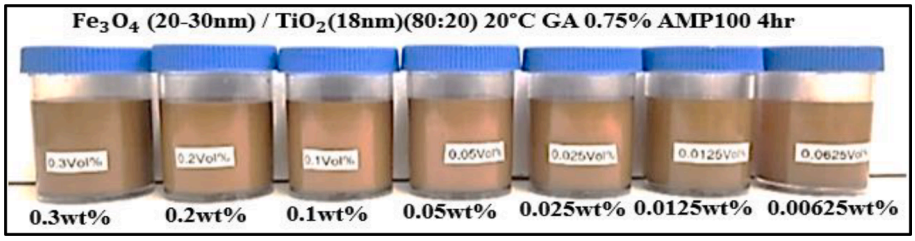

Fig. 2. Visual observation of Fe_3O_4/TiO_2 nanofluids.

Scanning Electron Microscopy (SEM) imaging. The morphological characteristics of Fe_3O_4 and TiO_2 (18 nm) nanoparticles were observed in SEM images presented in Fig. 3. These images were captured at a magnification of 100 KX, with an EHT of 2.0 kV, and a scanning speed of 9 μm/s. the Fe_3O_4 image illustrates a mix of small and large dispersed plate-like nanosheets. Additionally, the spherical shapes of TiO_2 (18 nm) nanoparticles and the last SEM image Fe_3O_4/TiO_2 of reveals the successful suspension of nanoparticles, indicating the formation of a stable nanofluid. In the TEM image, it is evident that Fe_3O_4 nanoparticles appear more distinct compared to Ti O_2.

2.6. Investigating thermo-physical properties of magnetic hybrid nanofluids

To assess the stability of the nanofluids, a method similar to previous studies Giwa et al. [35], and Osman et al. [36]. was employed. A data logger with a viscosity meter was set up to record data at 5-minute intervals over 10 h, as shown in Fig. 4a, to evaluate stability at a temperature of 30 degrees. Visual inspections were conducted during a 30-day monitoring period. Over this period, no sedimentation was observed for nanofluids with volumetric fractions of 0.00625 % Vol, 0.0125 % Vol, and 0.025 % Vol, while slight settling was noticeable for 0.05 %Vol. In contrast, nanofluids with volumetric fraction of 0.3 % Vol, 0.2 % Vol, and 0.1 % Vol displayed signs of settling. These findings corroborate results reported by Krishnan et al. [37] UV–Vis spectroscopy, following Beer-Lambert's law [38,39] demonstrated a correlation between the absorption rate in Fe_3O_4/Ti O_2 nanofluids and particle volumetric fraction, as shown in Fig. 4b and 4c. The UV–Vis spectroscopy results indicate that lower absorption rates are associated with decreased particle volumetric fraction, which is, in turn, linked to sedimentation percentages. Over 30 days, substantial settling was observed for nanofluids with volume fractions of 0.3 % Vol, 0.2 % vol, and 0.1 % vol, with sedimentation factor (SF) percentages of 37.79 %, 35.43 %, and 31.79 %, 11.88 %, and 11.61 %, respectively. In contrast, nanofluids with volume fractions of 0.00625 % vol, 0.0125 % Vol, and 0.025 % vol exhibited exceptional stability, with SF percentages of 8.89 %, 9.82 %, and 10.24.%, respectively, highlighting their commendable stability, 0.05 % vol is 10.68 % is slightly stable, and 0.1 %, 0.2 %, and 0.3 % are less stable, suggesting the need for optimization and stabilizers, especially at higher concentrations.

Fig. 5a, presents the viscosity of the MHNFs over a temperature from 10 °C to 50 °C, offering a comparison with the viscosity of DIW. The viscosity of the MHNFs is observed to decrease with an increase in temperature However, it is worth noting that both thermal and electrical conductivity demonstrate an increase as the volume fraction of nanofluids rises, These findings corroborate results reported by Zadkhast et al. [40] and Oraon et al. [41], as shown in Fig. 5**b and 5c**. Simultaneously, Fig. 5d displays a decline in the pH levels of the nanofluids as the temperature elevates Higher nanoparticle concentrations at each temperature point further reduce the pH, indicating increased acidity. This contrasts with DIW, which maintains a relatively constant pH around 7, emphasizing the significant impact of nanoparticles on fluid pH and suggesting complex physicochemical interactions as temperature and concentration vary, aligning with the patterns identified in prior studies by Krishnan et al. [37], and Giwa et al. [35]. These findings show nanofluids' complex and multifaceted nature, highlighting the critical importance of meticulously selecting the most appropriate concentration for specific applications.

2.7. Experimental setup for force CHT and method

Fig. 6**a and b** illustrate the experimental setup and the test rig layout, including a pressure transducer, a storage tank, a micro gear pump, a DC power supply, a tube-in-tube heat exchanger, a test section, thermocouples, a flow meter, and a data acquisition system. This setup is designed to study the heat transfer properties of nanofluids. A Constantine heating wire wraps around the test section to supply heat, and thick insulation minimizes heat loss. Nanofluids with varying weight concentrations are pumped through a copper pipe, and their mass flow rate is measured using a flow meter. The inlet temperature is kept at 20 °C by cooling the heated nanofluids through a heat exchanger, which transfers heat to cold water using a circulation pump. The data acquisition system collects and processes signals from the flow meters, pressure transducers, thermocouples, and the power supply.

In Fig. 6**c**, the testing portion comprises a copper tube that is circular, 1500 mm in length, with an inner diameter of 8 mm and an outer diameter of 9.5 mm. Four strategically placed thermocouples monitor tube wall temperatures at regular 130 mm intervals in North, South, East, and West directions. Continuous temperature monitoring occurs at the nanofluid inlet and outlet. A 200 W Constantine wire provides a constant heat flux, powered by a DC source with 1.22 A and 180 V. The shorter, 1000 mm long test section ensures fully developed hydraulics. Data accuracy is maintained by repeating experiments thrice, and calculations use the average wall temperature.

The thermophysical characteristics of the MHNFs were assessed, and the density, as well as specific heat of each MHNF, were determined using Pak and Cho's theoretical framework [42], as represented in Eqs. (3) and (4).

$$\rho_{nf} = (1-\varphi)\rho_{bf} + \varphi\rho_{np} \tag{3}$$

$$C_{pnf} = \frac{(1+\varphi)\rho_{bf}C_{pbf} + \varphi\rho_{np}C_{pnp}}{(1-\varphi)\rho_{bf} + \varphi\rho_{np}} \tag{4}$$

where, φ denotes mass ratio NF, and ρ_{nf}, ρ_{bf}, and $\varphi\rho_{np}$ stand for the densities of the nanofluid, base fluid, and nanoparticles, respectively. Additionally, C_{pnf}, C_{pbf}, and C_{pnp} denote their respective specific heats. The calculation of specific heat and density for MHNFs of Fe_3O_4/Ti O_2 is performed using Eqs. (5) and (6) [43]

$$\rho_{np} = \frac{\varphi_1\rho_{np1} + \varphi_2\rho_{np2}}{\varphi} \tag{5}$$

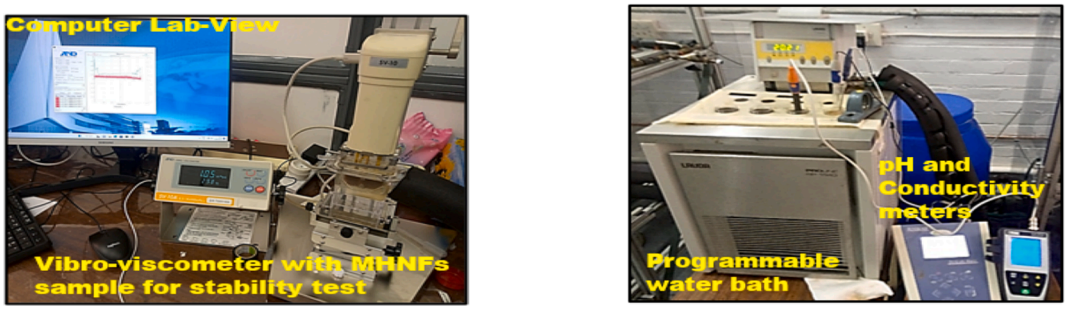

Fig. 3. SEM Morphology Investigation: (a) **Fe_3O_4** (20–30 nm) and (b) **TiO_2** (18 nm) Nanoparticles (c) Hybrid of **Fe_3O_4/TiO_2**.

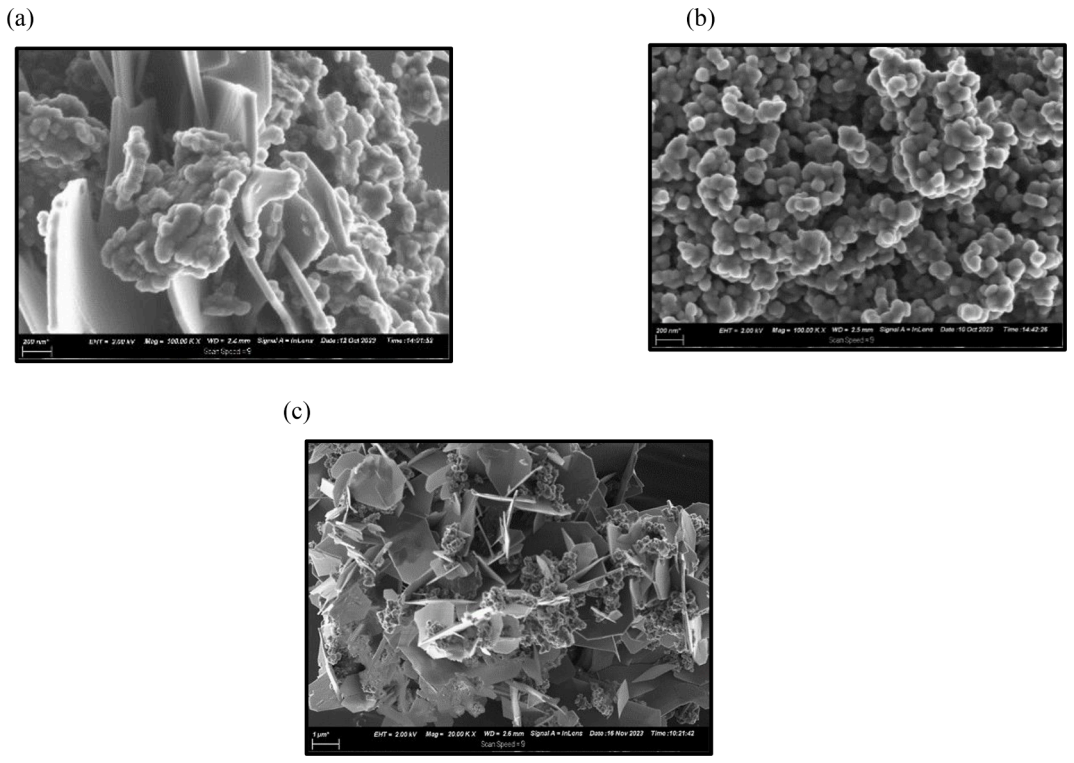

Fig. 4. (a) Evaluation of stability as a function of time (b) Effect of Fe_3O_4/TiO_2/DW density on light absorption at different wavelengths (c) Effect of Fe_3O_4/TiO_2/DW density on light absorption at different wavelengths.

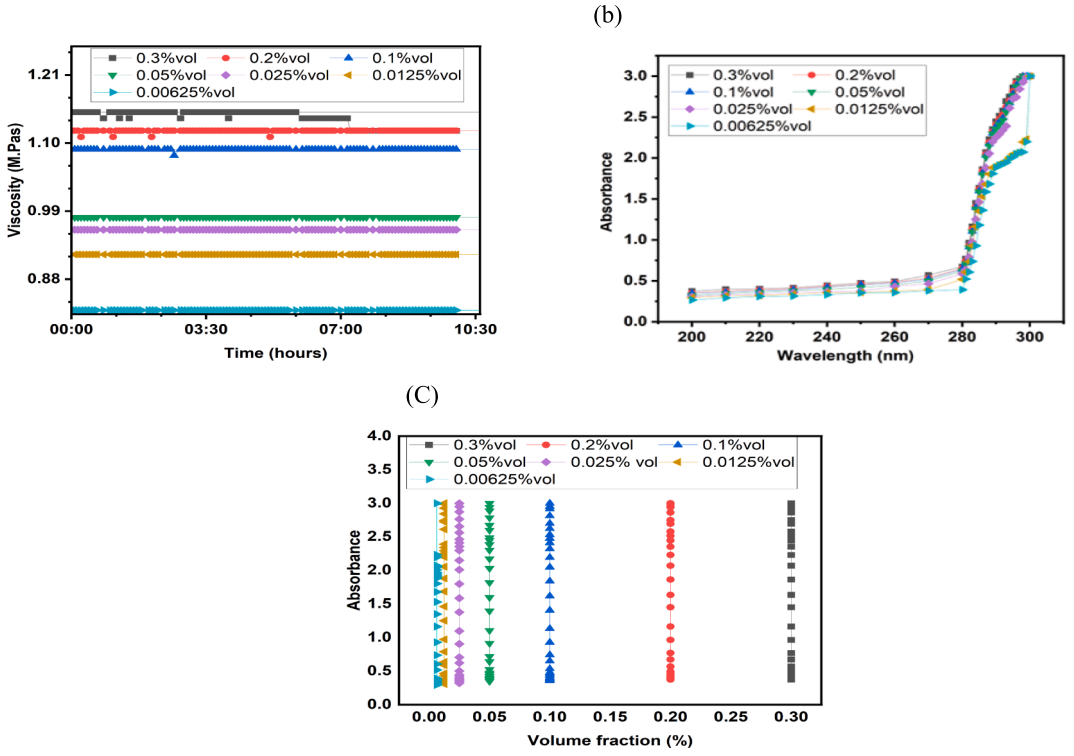

Fig. 5. (a) Influence of temperature on viscosity (b) Temperature-dependent on electrical conductivity (c) Temperature-dependent on thermal conductivity (d) Influence of temperature on pH.

$$C_{pnf} = \frac{\varphi_1 \rho_{np1} C_{pnp1} + \varphi_2 \rho_{np2} C_{pnp2}}{\rho_{np} \varphi} \quad (6)$$

The analysis of CHT and Nusselt number at various volume fractions involves utilizing thermophysical properties. Specifically, this entails estimating the heat absorption of the working fluid and the energy supplied to the test section, as described by Eqs. (7) and (8) [44]

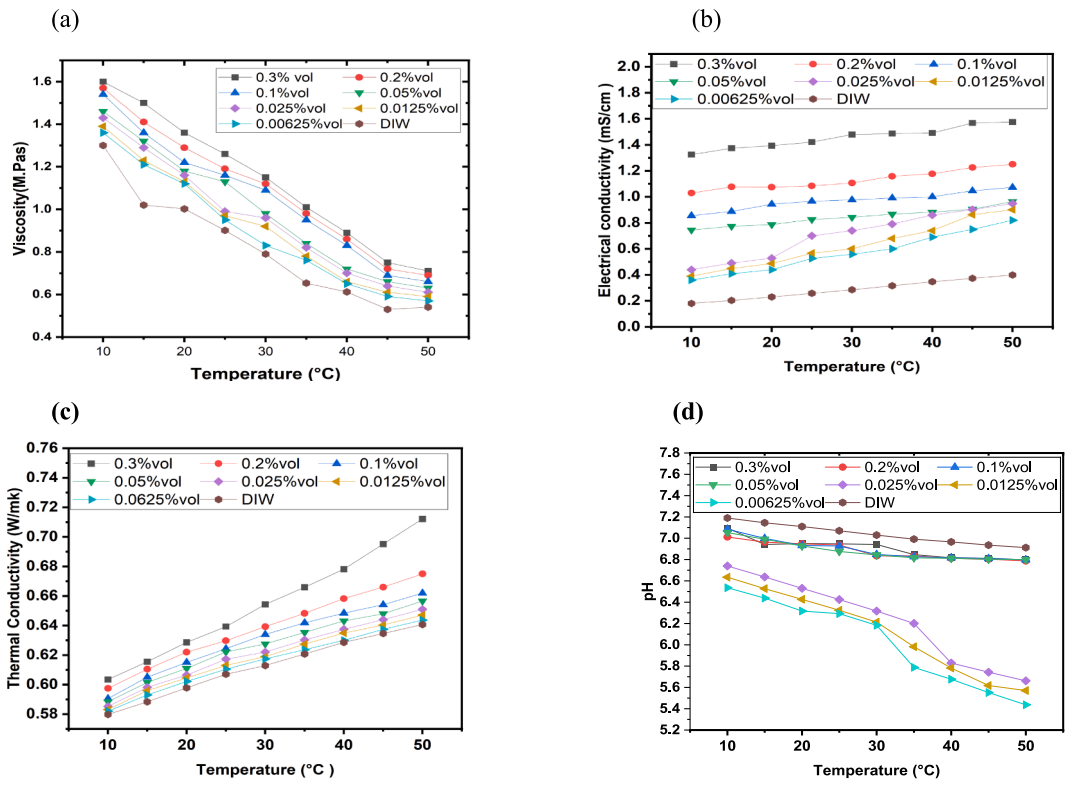

Fig. 6. (a) Schematic diagram set-up (b) Picture of test rig (c) Schematic diagram of the test section.

$$P = VI \tag{7}$$

$$Q = \dot{m}c(t_O - t_i) \tag{8}$$

where V represents voltage, I stands for the current supplied by the power source, $\dot{m}$ and c denote the mass flow rate and specific heat of the working fluid, respectively. $t_O and t_i$ correspond to the outlet and inlet temperatures of the test section, respectively. Utilizing Eq. (9) [45], computations are conducted to ascertain the local CHT coefficient along the axial distance of the test section.

$$\mathrm{h} = \frac{\mathrm{Q}}{A(t_w - t_b)} \tag{9}$$

To ascertain the local CHT coefficient at every thermocouple point, the bulk fluid temperature was computed by utilizing the inlet and outlet temperatures, specific heat, and heat flux information obtained from a flow meter. Comparing this with the thermocouple-recorded surface temperature allowed computation of the Nu. The Nu was calculated using the obtained CHT coefficient from Eq. (10) [46] and the measured thermal conductivity of the nanofluid.

$$\mathrm{Nu} = \frac{\mathrm{hD}_i}{\mathrm{k}} \tag{10}$$

where A represents the test section's area, t_w signifies the average wall temperature, t_b and stands for the average bulk temperature, the Nu is directly related to the CHT, as demonstrated by Eq. (10). where, D_i represents the inlet diameter of the test section, and K corresponds to the thermal conductivity of the nanofluids.

Besides performing heat transfer measurements, the research also encompassed assessing viscous pressure losses in the test section for deionized water and nanofluids. The experimental results were then contrasted with projected pressure loss estimates in Eq. (11) [46]

$$f = \frac{\Delta P}{\left(\frac{L}{D_i}\right)\left(\frac{\rho v^2}{2}\right)} \tag{11}$$

Before investigating nanofluid convective heat transfer coefficients, we validated our setup by testing it with DIW in a circular tube Re 3200–55,000. We compared our results to Ghajar and Tam (1994) [47] and Olivier and Meyer [48] equations, suitable for turbulent flows in Eqs. (12) and (13).

$$\mathrm{Nu} = 0.026.Re^{0.8}.Pr^{0.385}.\left(\frac{x}{D}\right)^{-0.0054}\left(\frac{u}{u_w}\right)^{0.4} \tag{12}$$

$$3 \le \frac{x}{D} \le 192; 7000 \le 49000; 4 \le Pr \le 34; 1.1 \le \frac{u}{u_w} \le 1.7$$

$$\mathrm{Nu} = 0.026.Re^{0.788}.Pr^{\frac{1}{3}}.\left(\frac{u_b}{u_w}\right)^{0.4} \tag{13}$$

With the range of $3.73 \le \mathrm{Pr} \le 5.06$ and $3000 \le \mathrm{Re} \le 17{,}800$.

In Fig. 7, the Current experimental Nu are compared to Olivier and Meyer's correlation, with an average deviation of 0.47 % (highest 6.6 %) in a turbulent flow. Ghajar and Tam's correlation shows a 3.4 % average deviation (highest 10.5 %) in turbulent flow. The results closely match experiments with DIW.

2.8. Data reduction and uncertainty

The methodology outlined by Dunn [49], was employed to compute the uncertainties associated with both the measured and evaluated parameters. These uncertainties were assessed at a 95 % confidence level as shown in Eq. (14).

$$u_x = \sqrt{u_B^2 + U_P^2}, P\% \tag{14}$$

(a)

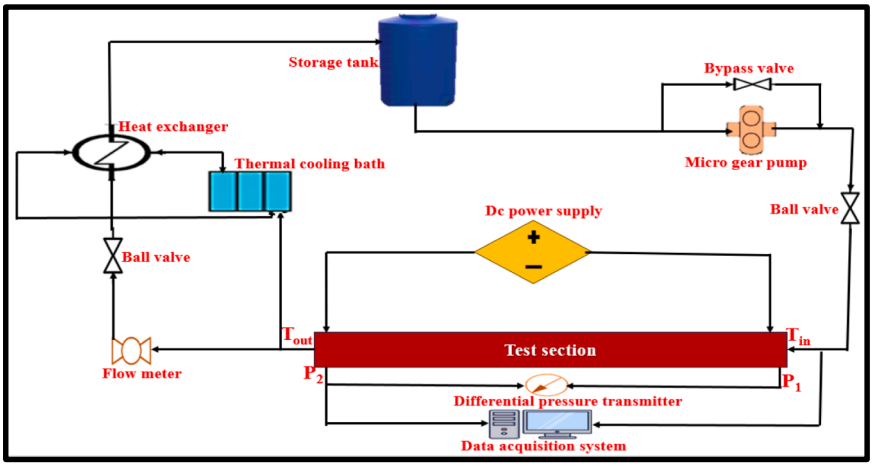

(b)

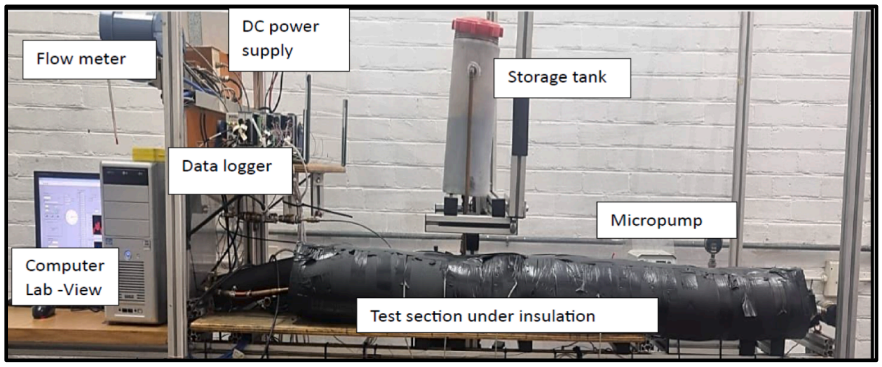

(c)

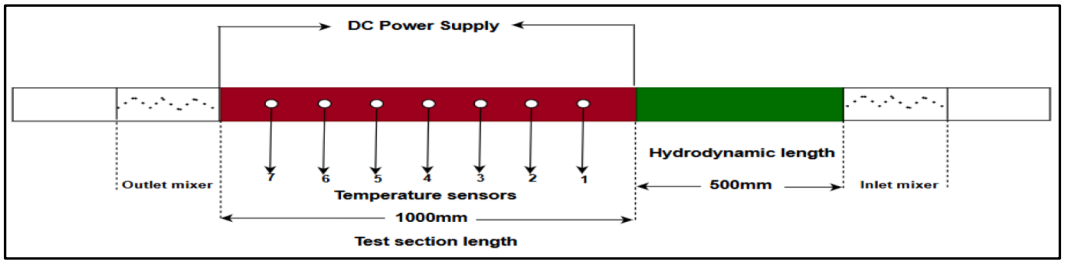

Fig. 7. Validation of experimental setup.

where u_B represents bias error and u_p represents the precision error in x with a probability of P%.

The calculation of parameter uncertainty based on measured variables can be accomplished using a series of equations as outlined below in 15 to 17,

$$R(x) = f(x_1, x_2, x_3, \cdots\cdots\cdots x_n) \tag{15}$$

For a given variable x_i, the uncertainty in the parameter R, concerning both its mean value $\overline{R}$ and its true (actual) value R_{actual}, can be expressed as follows,

$$R_{actual} = \overline{R} + \delta R \tag{16}$$

where δR is the uncertainty in R can be expressed as follows,

$$\delta R = \sqrt{\left(\delta_{x1}\frac{\partial R}{\partial_{x1}}\right)^2 + \left(\delta_{x2}\frac{\partial R}{\partial_{x2}}\right)^2 + \cdots\cdots\cdots + \left(\delta_{xn}\frac{\partial R}{\partial_{xn}}\right)^2} \tag{17}$$

Where δ_{x_i} represents the uncertainty of the evaluated variable x_i.

The uncertainty of the CHT coefficient in the experimental outcomes was approximately 0.116 %, which falls well within an acceptable range. This low level of uncertainty underscores the reliability and precision of the experimental measurements, ensuring that the reported enhancements in heat transfer are both accurate and reproducible.

Table 2 displays the uncertainty associated with the experimental outcomes, illustrating the widest range of uncertainties associated with each parameter across all conducted experiments.

Table 2
The measured uncertainties in the parameters.

Parameter	Uncertainty (%)
Reynolds number	2.145
Bulk temperature	1.2
CHT coefficient, h	2.49
Nusselt number	3.69

3. Results and discussion

3.1. Heat transfer coefficient of varying volume fraction

Fig. 8 illustrates the effect of varying volume fractions on heat transfer at different Reynolds numbers with Fe_3O_4/TiO_2 nanofluid volume fraction, the percentage enhancements in the CHT coefficient for various volume fractions of Fe_3O_4/TiO_2 nanofluid, in comparison to DIW, exhibits a notable trend. At 0.3 % vol, the CHT coefficient experiences a substantial enhancement of approximately 11.42 %, while at 0.2 % vol, it increases by approximately 14.03 %. The enhancement continues to rise with decreasing volume fractions, reaching about 18.04 % at 0.1 %vol and approximately 19.98 % at 0.05 %vol. The enhancement is more pronounced for even lower concentrations, with approximately 22.91 % at 0.025 %vol and a peak of around 26.33 % at 0.0125 %vol. The enhancement remains high at 0.00625 % Vol, with an approximate increase of 24.30 %. These results demonstrate the significant improvements in CHT coefficient when using Fe_3O_4/TiO_2 nanofluid as compared to DIW for various volume fractions.

These results collectively emphasize the substantial improvements in CHT coefficient offered by Fe_3O_4/TiO_2 nanofluid at various volume fractions when compared to DIW, with an optimal enhancement observed at intermediate volume fractions. Contrary to the conventional belief that higher nanoparticle concentrations improve heat transfer, the data consistently demonstrates that the 0.00125 %vol concentration yields the highest heat transfer coefficient, followed by 0.025 %vol. This challenges common assumptions and suggests that lower nanoparticle concentrations are more effective in this specific nanofluid and flow regime. Possible reasons include improved nanoparticle dispersion, reduced viscosity, and better alignment with flow characteristics at 0.05 % concentration.

Fig. 8**b, c, and d** depict local CHT coefficients vs. position (x/d) for Fe_3O_4/TiO_2 nanofluid at various volume fractions and DIW as a reference at the lowest Re for turbulent flow in a circular pipe. Regardless of Re, 0.0125 %vol consistently achieves the highest heat transfer coefficients at various positions along the pipe, establishing it as the optimal concentration for enhancing heat transfer in this experimental setup. This holds across different flow x/d positions. Variations in heat transfer coefficients along the pipe length, regardless of Reynolds number, underscore non-uniform heat transfer. This highlights the need to consider specific positions (x/d) in applications requiring efficient heat transfer. Notably, at the of Re 3214.162, the 0.3 %vol concentration of $Fe_3O_4/Ti\ O_2$ nanofluid exhibited reduced heat transfer enhancement compared to DIW. A similar trend was seen with 0.2 %vol, and 0.1 %vol particularly at positions x/d 15 and 31.25, due to elevated fluid viscosity hindering $Fe_3O_4/Ti\ O_2$ nanofluid flow. These findings emphasize the complex nature of nanofluid behavior in heat transfer, influenced by multiple factors including nanoparticle properties, their interactions, and flow conditions.

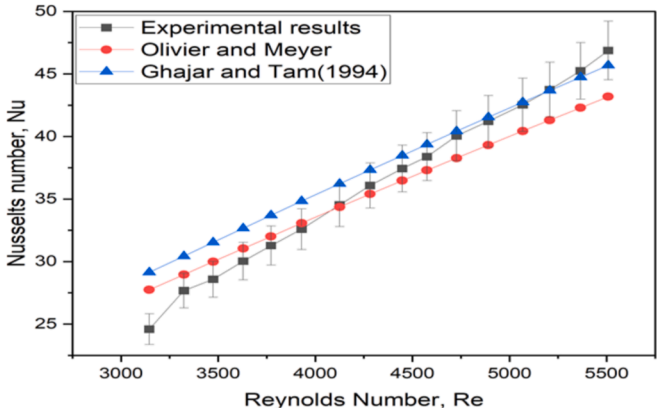

Fig. 8. (a) Effect of varying volume fractions on heat transfer at different Reynolds numbers and Other Fig. 8 Local CHT coefficients as a function of position (x/d) for **Fe_3O_4/Ti O_2** nanofluid at various volume fractions. (b) Highest (Re 5200) (c) Middle (Re 4200) (d)Lowest (Re 3200).

3.2. Percentage enhancements in volume fraction at various positions along the tube (x/d)

In Fig. 9**a**, At Re 5200, the $Fe_3O_4/Ti\ O_2$ nanofluid consistently exhibits positive percentage enhancements in volume fraction at various positions along the tube (x/d) for concentrations ranging from 0.3 %Vol to 0.00625 %Vol. The highest percentage enhancements, reaching approximately 46.24 % and 45.07 %, are typically observed at x/d at 96.25 for 0.00625 %Vol and 0.0125 %vol respectively and in contrast, the lowest percentage enhancements, going as low as approximately 6.24 %, are found at x/d is 80 for 0.3 %vol. challenging the common assumption that higher nanoparticle concentrations enhance heat transfer. Fig. 9**b**, At Re 4200, a similar pattern is observed, with positive values in most cases and percentage enhancements ranging from approximately 5–36.86 %. The highest enhancements occur at x/d is 47.5 for 0.0125 %Vol, while the lowest enhancements are at x/d 47.5 for 0.3 %vol, with a percentage of approximately 5 %. In Fig. 9**c**, at a Re of 3200, the percentage enhancements at various volume fractions (0.00625 %vol, 0.0125 %Vol, and 0.025 %vol) were examined. The percentage enhancements ranged from approximately 53.58–24.29 %. The most significant enhancements were observed at x/d 96.25 for the 0.025 %Vol volume fraction. However, no enhancements were detected for the 0.3 %Vol volumetric fraction at any position. For the 0.2 %Vol and 0.1 %Vol volume fractions, it is worth noting that there were no enhancements at x/d 15 and 31.25 positions.

In Fig. 10**a**, the mean heat transfer coefficient comparison between DIW and Fe_3O_4/TiO_2 nanofluid in a circular tube during forced convection reveals a noteworthy trend. Contrary to the conventional belief that higher nanoparticle concentrations improve heat transfer, the data consistently demonstrates that the 0.0125 %vol concentration yields the highest heat transfer coefficient, followed by 0.00625 %vol. This challenges common assumptions and suggests that lower nanoparticle concentrations are more effective in this specific nanofluid and flow regime. Possible reasons include improved nanoparticle dispersion, reduced viscosity, and better alignment with flow characteristics at 0.0125 %vol, 0.0062 %vol and 0.025 %vol concentration. This underscores the need for a nuanced approach to nanoparticle concentration and system-specific design for efficient heat transfer applications.

While in Fig. 10**b and 10c**, the pressure drops as a function of flow rate and the pressure drops as a function of Re as depicted. The pressure drops as a function of Re, the experimental outcomes proved the behaviour of Fe_3O_4/TiO_2 nanofluids in the turbulent region of forced convection is governed by a combination of factors, primarily concentration, viscous drag effects of the Fe_3O_4/TiO_2 nanofluids and flow rate. The findings show that as the nanofluid concentration increases, there is a correlated increase in pressure drop. This concentration-dependent behaviour is particularly pronounced at higher concentrations, highlighting the nanofluids' heightened influence on hydraulic resistance. Moreover, the relationship between pressure drops and flow rate for all concentrations is characterized by a linear decrease. Interestingly, this linear trend aligns closely with the behaviour of DIW, indicating that while flow rate remains the primary determinant, higher nanoparticle concentration exacerbates the pressure drop, the finding is in alignment

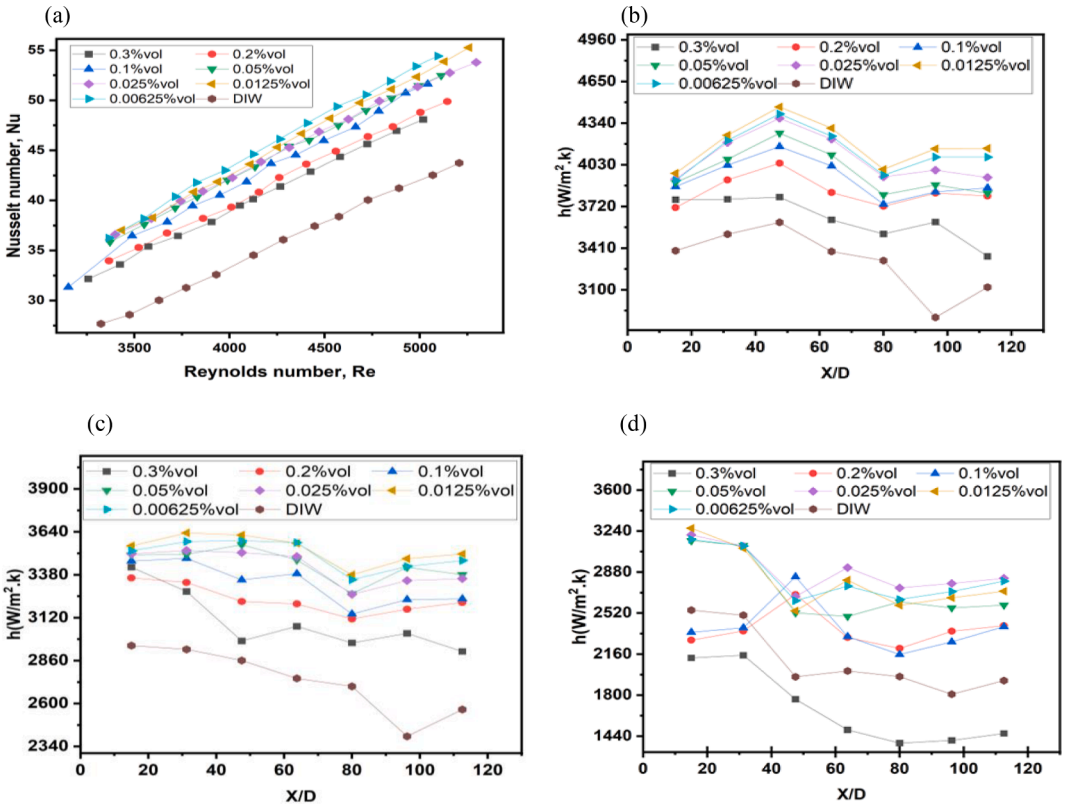

Fig. 9. Percentage enhancements for each volume concentration at various positions along the tube (x/d) (a) Highest (Re 5200) (b) Middle (Re 4200) (c)Lowest (Re 3200).

with Emad et al. [46,50] and Sundar [19]. While Fig. 10**c,** reveals a complex relationship with pressure drop at various concentrations compared to DIW. The pressure drop data across different Re and volumetric fractions of Fe_3O_4/TiO_2 nanofluid exhibits a clear linear trend. As nanoparticle concentration increases, the pressure drop consistently rises, indicating a direct relationship between concentration and hydraulic resistance. The highest pressure drops, approximately 21 %, occurs at Re 5018 for the 0.3 % vol fraction. Conversely, as the volume fraction decreases, the pressure drop diminishes, with lower concentrations corresponding to reduced pressure drops, such as 13.10 % at Re 5144.4 for 0.2 % vol and 7.67 % at Re 5258.7 for 0.0125 % vol. This linear behavior suggests that increased nanoparticle concentration leads to greater fluid viscosity, resulting in higher resistance to flow.

Moreover, flow rate plays a significant role, as higher Re values amplify the pressure drop due to the combined effects of turbulence and concentration, aligning with patterns observed in previous studies by Chinnasamy et al. [44], The implications of these results are significant while increasing nanoparticle concentration may seem beneficial for heat transfer, this study shows that lower volume fractions (0.0125 % vol and 0.00625 % vol) enhance heat transfer more effectively than higher concentrations. However, the data indicate that higher concentrations also introduce significant resistance within the system, impacting energy efficiency and challenging balancing the benefits of enhanced heat transfer against the drawbacks of higher-pressure losses.

Determining the optimal concentration that balances these challenges is crucial for applying nanofluids in thermal systems. Carefully selecting nanoparticle concentrations and flow rates is vital to optimize thermal performance while managing pressure drop, ensuring that the benefits outweigh the potential drawbacks.

In Fig. 10**d, e, and f**, pressure drop versus flow rate for Fe_3O_4/TiO_2 nanofluids at varying Re 52,000, 4200, and 3200 and different x/d positions and concentrations compared to DIW unveil a consistent relationship between volume fraction and pressure drop, indicating that lower concentrations lead to reduced pressure losses at various positions (x/d). Position specific variations are evident, where specific positions experience lower pressure drops, reflecting varying resistance levels and flow dynamics. Moreover, introducing substances increases pressure drop compared to DIW at all positions, emphasizing the trade-off between enhancing fluid properties and elevating pressure drop. The relationship between pressure drops and position underscores the intricate and dynamic nature of fluid flow within the system, offering crucial insights for applications prioritizing the minimization of pressure drops. These findings showcase a concentration-driven impact on pressure drop and its dependence on position within the system, providing valuable data for applications in fluid dynamics and system efficiency.

Furthermore, to assess the overall performance of Fe_3O_4/TiO_2 nanofluids in heat transfer systems and to determine the optimum volume fraction the Total Efficiency Index (TEI) was evaluated.

The TEI is a parameter used to evaluate the overall performance of Fe_3O_4/TiO_2 nanofluids in heat transfer systems, particularly when using nanofluids. It combines both the thermal enhancement, and the associated pressure drop or friction factor penalties into a single metric, providing a more comprehensive assessment of the system's efficiency.

The TEI is typically defined as the ratio of the heat transfer enhancement (often measured as the convective heat transfer ratio between the nanofluid and the base fluid) to the corresponding increase in pumping power or friction factor as express in Eq. (18) [51].

$$\eta = \frac{\frac{h_{avg,bf}}{h_{avg,nf}}}{\frac{\Delta P_{nf}}{\Delta P_{bf}}} \tag{18}$$

Fig. 11**a and b** show the analysis of the TEI for Fe_3O_4/TiO_2 nanofluids across various volume fractions, ranging from 0.00625 % to 0.3 %, reveals critical insights into the optimal nanoparticle concentration for heat transfer systems. The data indicates that lower concentrations, particularly around 0.0125 % vol, consistently exhibit higher TEI values

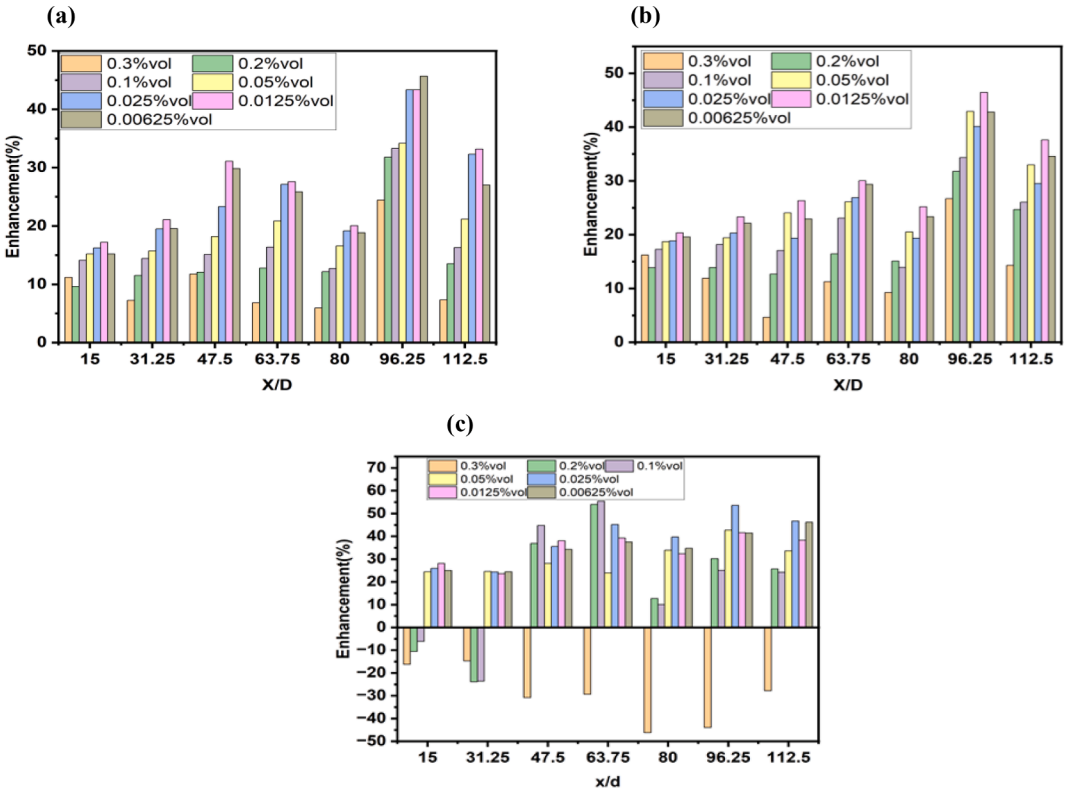

Fig. 10. (a)Comparison of mean heat transfer coefficient with flow rate for DW and Fe_3O_4/Ti O_2 nanofluid. (b)Pressure drops as a function of flow rate and (c) Pressure drop versus flow rate at varying Reynolds numbers for Fe_3O_4/Ti O_2 nanofluids at different x/d positions and concentrations (a) Highest (Re 5200) (b) Middle (Re 4200) (c)Lowest (Re 3200) (a) Highest (Re 5200), (b) Middle (Re 4200) (c)Lowest (Re 3200) (d) Pressure drop versus flow rate for Fe_3O_4/Ti O_2 nanofluids at Re 52,000 with different x/d positions and concentrations compared to DIW (e) Pressure drop versus flow rate for Fe_3O_4/Ti O_2 nanofluids at Re 42,000 with different x/d positions and concentrations compared to DIW (f) Pressure drop versus flow rate for Fe_3O_4/Ti O_2 nanofluids at Re 3200 with different x/d positions and concentrations compared to DIW.

across different flow rates. This suggests that as the concentration of nanoparticles decreases, the thermal efficiency improves, likely due to better nanoparticle dispersion and lower viscosity, which enhances convective heat transfer while minimizing thermal resistance and pumping power requirements.

In contrast, higher concentrations, especially in the range of 0.2–0.3 % vol, demonstrate significantly lower TEI values. This reduction in efficiency can be attributed to the increased thermal resistance and flow disruption caused by the higher presence of solid particles, which impede fluid movement and diminish overall heat transfer effectiveness. The mid-range concentrations, such as 0.05–0.1 % vol, show moderate TEI values, indicating some benefit in heat transfer but not as pronounced as at lower concentrations.

The optimal concentration for Fe_3O_4/Ti O_2 nanofluids is identified at approximately 0.0125 % vol, where the TEI is highest across all flow rates. This concentration offers the best balance between enhanced heat transfer and minimal pressure drop, making it ideal for applications requiring efficient thermal performance. The implications for heat transfer systems are significant, as this concentration can improve energy efficiency by maximizing heat transfer rates while minimizing the additional energy required for pumping. In practical applications such as heat exchangers or cooling systems, utilizing a nanofluid with 0.0125 % vol concentration could lead to more energy-efficient operations, reducing operational costs and optimizing system performance. Therefore, this concentration should be considered the optimal choice for engineers and designers aiming to achieve high-efficiency thermal management in various industrial applications.

Table 3 presents a comparison of the current study's findings with similar research in the literature, emphasizing the novelty of the Fe_3O_4/TiO_2/DIW hybrid magnetic nanofluid. Unlike previous studies, which reported maximum heat transfer enhancements at higher nanoparticle concentrations, this study demonstrates significant improvements even at lower concentrations. Specifically, an enhancement of 26.33 % was observed at 0.0125 % volume fraction and 24.30 % at 0.00625 % volume fraction under turbulent flow. This contrasts with earlier work, such as Lee et al. [52], who found a 23 % increase at 0.2 wt % for $Co_{0.5}Zn_{0.5}F_2O_4$/DIW, and Sundar et al. [19], who reported a 31 % enhancement at 0.3 wt% for Fe_3O_4/MWCNT/DIW. The results underline the effectiveness of Fe_3O_4/Ti O_2/DIW in achieving high heat transfer performance at lower nanoparticle concentrations.

4. Conclusion

This study investigates the optimal nanoparticle concentration for Fe_3O_4/Ti O_2 hybrid nanofluids with an 80:20 ratio under turbulent flow conditions. The aim was to balance enhanced convective heat transfer with minimized pressure drop and energy consumption. Existing research has often focused on single nanofluids or hybrid nanofluids under laminar conditions, emphasising high nanoparticle concentrations. This approach can lead to increased viscosity and higher energy requirements, thus creating a need for more effective optimization of nanoparticle concentrations.

Key Findings of Fe_3O_4/TiO_2 nanofluid presents a multifaceted picture of its behaviour.

1. Nanofluid Stability: The stability of Fe_3O_4/TiO_2 nanofluids was assessed, revealing that nanofluids with lower volume fractions (0.00625 %Vol, 0.0125 %Vol, and 0.025 %Vol) exhibited exceptional stability over a 30-day monitoring period. In contrast, those with higher volumetric fractions (0.1 %Vol, 0.2 %Vol, and 0.3 %Vol)

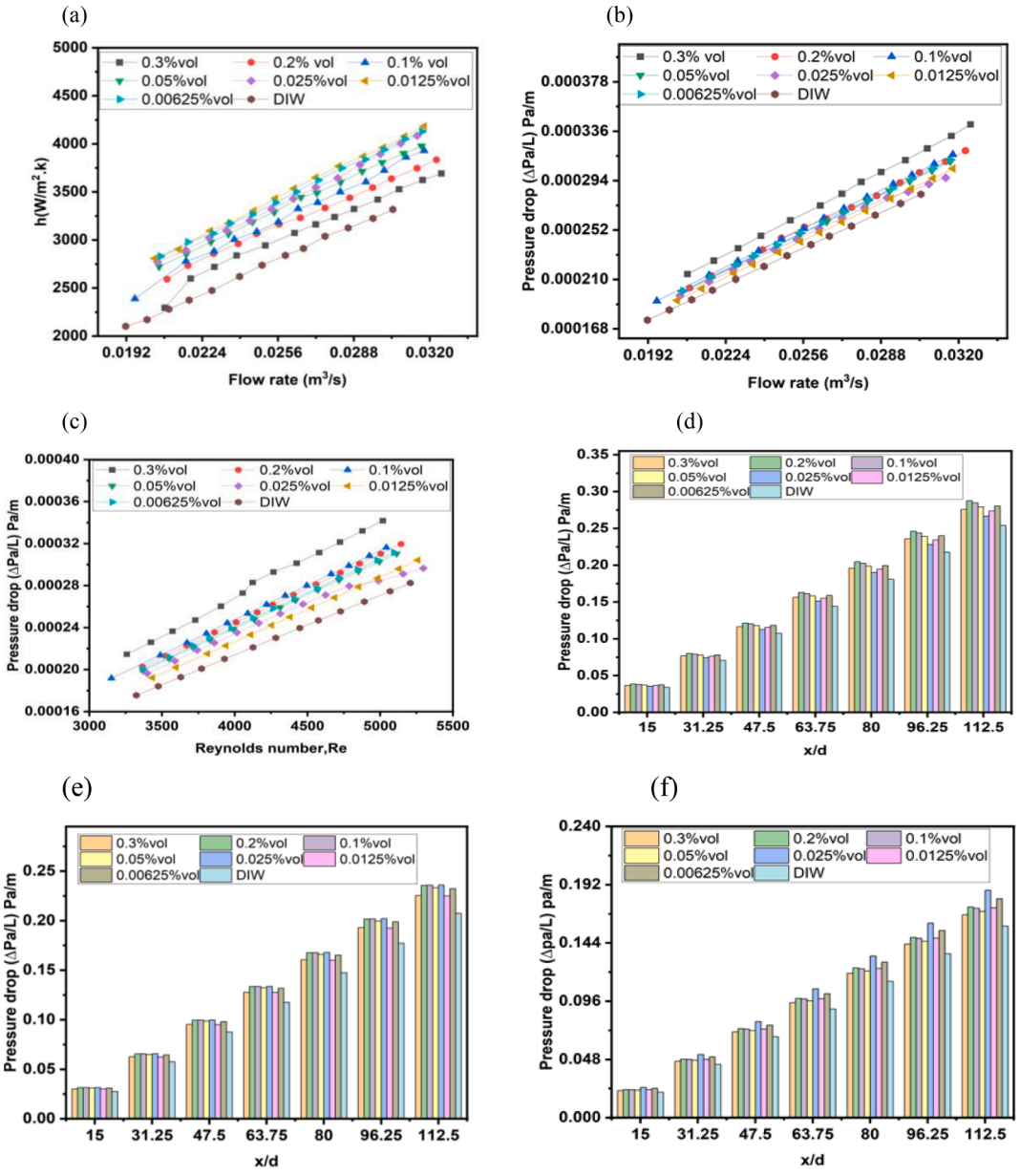

Fig. 11. (a) Total efficiency index of Fe_3O_4/Ti O_2 nanofluids across various volume fractions and Reynolds (b) Total efficiency index of Fe_3O_4/Ti O_2 nanofluids across various volume fractions and flow rates.

Table 3
Comparison of CHT in magnetic nanofluids with current study versus similar literature.

Investigator	Nanofluid type	Flow regime	concentration	Observation
Lee et al. [52]	$Co_{0.5}Zn_{0.5}F_2O_4$/DIW	Laminar	0.025–0.2 wt%	CHT Coefficient increases with a maximum of 23 % at 0.2 wt%
Shahsavar et al. [53]	Fe_3O_4/CTNs/DIW	Laminar	0.5–0.9 wt%	CHT Coefficient increment with a maximum of 20.5 % at 0.5 wt%
Chinnasamy et al. [44]	Fe_3O_4/MWCNT/DIW	Laminar	0.025–0.2 wt%	The highest increment was 15.9 % at 0.1 wt%
Lee et al. [54]	Fe_3O_4/MWCNT/DIW/EG	Laminar	0.025–0.2 wt%	The highest improvement was 3.23 % at 0.1 wt%
Tekir et al. [55]	Fe_3O_4/Cu/DIW	Laminar	0.5–1.5 wt%	CHT Coefficient increment with a maximum of 10.5 % at 1.5 wt%
Sunder et al. [19]	Fe_3O_4/MWCNT/DIW	Turbulent	0.1–0.3 wt%	Maximum of 31 % enhancement in Nu at Re 22,000 with 0.3 wt% at 1.18 times increment in pumping power
Current study	Fe_3O_4/TiO_2/DIW	Turbulent	0.00625–0.3 wt %	An enhancement at the lower volume fraction of 26.33 % at 0.0125 % vol, and 24.30 % at 0.00625 % vol

displayed signs of settling. This underscores the importance of selecting the appropriate nanoparticle concentration to maintain stability in nanofluid applications

2. Uv–vis spectroscopy and Sedimentation: UV–Vis spectroscopy was employed to analyse nanofluid stability. It was found that lower absorption rates correlated with decreased particle volume fractions, which, in turn, were linked to sedimentation percentages. These findings align with previous studies and highlight the complex nature of nanofluids
3. Heat transfer Enhancement: The coefficient of CHT in the nanofluids demonstrated significant improvements with increasing particle volume fraction, up to an optimal concentration of 0.0125 % vol. Contrary to conventional beliefs, lower nanoparticle concentrations proved to be more effective in enhancing heat transfer, possibly due to factors such as improved nanoparticle dispersion, reduced viscosity, and better alignment with flow characteristics
4. Viscosity and Conductivity: The viscosity of the MHNFs decreases with rising temperature, aligning with typical fluid behavior. Both thermal and electrical conductivity increase with the volume fraction of nanofluids, indicating their potential to enhance these properties compared to deionized water (DIW)
5. pH Levels: The results reveal a decline in the pH levels of the nanofluids as the temperature rises. Higher nanoparticle concentrations result in further reductions in pH, indicating increased acidity. This contrasts with the relatively constant pH of DIW, underscoring the complex physicochemical interactions within the nanofluids
6. CHT coefficient Enhancement: Demonstrates a significant improvement in the CHT coefficient with varying volume fractions of Fe_3O_4/Ti O_2 nanofluid, compared to DIW. An optimal enhancement is observed at lower volume fractions, challenging the common assumption that higher nanoparticle concentrations always lead to better heat transfer. Lower concentrations are more effective, likely due to factors like improved nanoparticle dispersion, reduced viscosity, and better alignment with flow characteristics
7. Pressure drops are highest at 21 % for 0.3 % vol at Re 5018, decreasing with lower concentrations: 13.10 % at Re 5144.4 (0.2 % vol), 11.94 % at Re 5041.6 (0.1 % vol), 9.82 % at Re 5112.2 (0.05 % vol), 7.67 % at Re 5258.7 (0.0125 % vol), and 10.29 % at Re 5094.0 (0.00625 % vol). The implications of these results are significant while increasing nanoparticle concentration may seem beneficial for heat transfer, this study shows that lower volume fractions (0.0125 % vol and 0.00625 % vol) enhance heat transfer more effectively than higher concentrations. However, the data indicate that higher concentrations also introduce significant resistance within the system, impacting energy efficiency and challenging balancing the benefits of enhanced heat transfer against the drawbacks of higher-pressure losses
8. The Total efficiency index (TEI) analysis of Fe_3O_4/Ti O_2 nanofluids across varying volume fractions reveals that the optimal nanoparticle concentration for achieving maximum thermal efficiency lies at approximately 0.0125 % vol. At this concentration, the nanofluids consistently exhibit higher TEI values, indicating enhanced heat transfer performance with minimal thermal resistance and pressure drop. The superior performance at this concentration is likely due to the more uniform dispersion of nanoparticles, which promotes effective convective heat transfer while maintaining low viscosity and reducing the pumping power required. Consequently, this concentration represents the most effective balance between thermal enhancement and system efficiency, making it the optimal choice for heat transfer applications

Conversely, higher concentrations, particularly between 0.2 % and 0.3 % Vol, demonstrate significantly lower TEI values, indicating a decrease in thermal efficiency. The presence of higher solid particle concentrations disrupts fluid flow, increasing thermal resistance and reducing overall heat transfer effectiveness. These findings underscore the importance of selecting the appropriate nanoparticle concentration to optimize thermal efficiency in heat transfer systems. By choosing the optimal concentration, engineers can achieve significant energy savings and improved system performance, making TEI a critical parameter in designing and operating advanced thermal management systems.

5. Implications and Recommendations

While this study has demonstrated the potential of Fe_3O_4/TiO_2 hybrid nanofluids at lower concentrations can provide superior thermal performance and energy efficiency compared to higher concentrations. This challenges the common assumption that more nanoparticles always lead to better heat transfer. For practical applications, selecting the optimal concentration is crucial for balancing thermal performance and system efficiency.

Further research is needed to explore different nanoparticle materials and hybridization ratios across various flow regimes. Additionally, investigating long-term stability and thermal conductivity under varying conditions could provide deeper insights into practical applications. Advanced modeling techniques, including machine learning, could optimize the properties of hybrid nanofluids, supporting their use in complex industrial systems.

6. Credit author contributions

Victor Omoefe Adogbeji: Contributed to data acquisition, experimental work, validation, results interpretation and drafted the original manuscript.

Mohsen Sharifpur: Methodology, validation, manuscript writing, and editing; supervised the research and secured funds.

Josua P. Meyer: Contributed to methodology, reviewed and edited the manuscript, and co-supervised the project.

Declaration of competing interest

The authors declare that they have no known competing financial interests or personal relationships that could have appeared to influence the work reported in this paper.

Data availability

Upon request, the data can be provided. approach, necessitating further research for comprehensive understanding and optimization in diverse practical applications.

References

[1] S.U.S. Choi, J.A. Eastman, Enhancing thermal conductivity of fluids with, ASME Int. Mech. Eng. Congr. Expo. 66 (1995) 99-105. https://doi.org/10.1115/1.1532008.
[2] C.H. Peng, Y.X. Liu, L.Z. Zhang, Radiation-convective heat transfer and performance analysis of a parallel-plates duct direct absorption solar heat collection system, Appl. Therm. Eng. 245 (2024) 122796, https://doi.org/10.1016/J.APPLTHERMALENG.2024.122796.
[3] M. Ahmed, M. Eslamian, Laminar forced convection of a nanofluid in a microchannel: Effect of flow inertia and external forces on heat transfer and fluid flow characteristics, Appl. Therm. Eng. 78 (2015) 326–338, https://doi.org/10.1016/J.APPLTHERMALENG.2014.12.069.
[4] S. Nasir, A. Berrouk, Z. Khan, Efficiency assessment of thermal radiation utilizing flow of advanced nanocomposites on riga plate, Appl. Therm. Eng. 242 (2024) 122531, https://doi.org/10.1016/J.APPLTHERMALENG.2024.122531.
[5] L. Shi, Y. Hu, Y. He, Magnetocontrollable convective heat transfer of nanofluid through a straight tube, Appl. Therm. Eng. 162 (2019), https://doi.org/10.1016/j.applthermaleng.2019.114220.
[6] Z. Narankhishig, J. Ham, H. Lee, H. Cho, Convective heat transfer characteristics of nanofluids including the magnetic effect on heat transfer enhancement - a review, Appl. Therm. Eng. 193 (2021), https://doi.org/10.1016/j.applthermaleng.2021.116987.
[7] S. Vinod, J. Philip, "Thermal and rheological properties of magnetic nanofluids: Recent advances and future directions," *Adv. Colloid Interface Sci.* 307. Elsevier B. V., Sep. 01, 2022. doi: 10.1016/j.cis.2022.102729.

[8] L.J. Felicia, S. Vinod, J. Philip, Recent advances in magnetorheology of ferrofluids (Magnetic Nanofluids)—a critical review, J. Nanofluids 5 (1) (2015) 1–22, https://doi.org/10.1166/jon.2016.1203.

[9] A.A. Karamallah, A. Habeeb Askar, L. Habeeb, The effect of magnetic field with nanofluid on heat transfer in a horizontal pipe investment cost analysis view project how to use engineering equation solver (EES): refrigeration and heat transfer applications view project the effect of magnetic field, Al-Khwarizmi Eng. J. 12 (3) (2016) 99–109.

[10] L. Sha, Y. Ju, H. Zhang, The influence of the magnetic field on the convective heat transfer characteristics of Fe3O4/water nanofluids, Appl. Therm. Eng. 126 (2017) 108–116, https://doi.org/10.1016/j.applthermaleng.2017.07.150.

[11] A.M. Ajeena, I. Farkas, P. Víg, Energy and exergy assessment of a flat plate solar thermal collector by examine silicon carbide nanofluid: An experimental study for sustainable energy, Appl. Therm. Eng. 236 (Jan. 2024) 121844, https://doi.org/10.1016/J.APPLTHERMALENG.2023.121844.

[12] G. Yıldız, Investigating the impacts of using TiO2-ZnO/POE hybrid nanolubricant in a heat pump system: An experimental study, Appl. Therm. Eng. 241 (2024) 122377, https://doi.org/10.1016/J.APPLTHERMALENG.2024.122377.

[13] R. Fu, Z. Liu, Y. Chen, Y. Yan, "Experimental investigation of turbulent forced heat transfer of Fe3O4 ethylene glycol – Water nanofluid with highly disaggregated particles," Therm. Sci. Eng. Prog. 10(October) (2018) 1–9. doi: 10.1016/j.tsep.2019.01.001.

[14] L.S. Sundar, H.M. Abebaw, M.K. Singh, A.M.B. Pereira, A.C.M. Sousa, Experimental heat transfer and friction factor of Fe3O4 magnetic nanofluids flow in a tube under laminar flow at high prandtl numbers, Int. J. Heat Technol. 38 (2) (2020) 301–313, https://doi.org/10.18280/ijht.380204.

[15] L. Syam Sundar, M.T. Naik, K.V. Sharma, M.K. Singh, T.C. Siva Reddy, "Experimental investigation of forced convection heat transfer and friction factor in a tube with Fe 3O 4 magnetic nanofluid," Exp. Therm. Fluid Sci., 37 (2012) 65–71, doi: 10.1016/j.expthermflusci.2011.10.004.

[16] S. Askari, H. Koolivand, M. Pourkhalil, R. Lotfi, A. Rashidi, Investigation of Fe3O4/Graphene nanohybrid heat transfer properties: experimental approach, Int. Commun. Heat Mass Transf. 87 (2017) 30–39, https://doi.org/10.1016/j.icheatmasstransfer.2017.06.012.

[17] J. Alsarraf, R. Rahmani, A. Shahsavar, M. Afrand, S. Wongwises, M.D. Tran, Effect of magnetic field on laminar forced convective heat transfer of MWCNT–Fe3O4/water hybrid nanofluid in a heated tube, J. Therm. Anal. Calorim. 137 (5) (2019) 1809–1825, https://doi.org/10.1007/s10973-019-08078-y.

[18] M. Asfer, B. Mehta, A. Kumar, S. Khandekar, P.K. Panigrahi, Effect of magnetic field on laminar convective heat transfer characteristics of ferrofluid flowing through a circular stainless steel tube, Int. J. Heat Fluid Flow 59 (2016) 74–86, https://doi.org/10.1016/j.ijheatfluidflow.2016.01.009.

[19] L.S. Sundar, M.K. Singh, A.C.M. Sousa, Enhanced heat transfer and friction factor of MWCNT-Fe3O4/water hybrid nanofluids, Int. Commun. Heat Mass Transf. 52 (2014) 73–83, https://doi.org/10.1016/j.icheatmasstransfer.2014.01.012.

[20] M. Yarahmadi, H. Moazami Goudarzi, and M. B. Shafii, "Experimental investigation into laminar forced convective heat transfer of ferrofluids under constant and oscillating magnetic field with different magnetic field arrangements and oscillation modes," Exp. Therm. Fluid Sci., 68 (2015) 601–611. doi: 10.1016/j.expthermflusci.2015.07.002.

[21] A. Abadeh, M. Sardarabadi, M. Abedi, M. Pourramezan, M. Passandideh-Fard, M. J. Maghrebi, Experimental characterization of magnetic field effects on heat transfer coefficient and pressure drop for a ferrofluid flow in a circular tube, J. Mol. Liq. 299 (2020), https://doi.org/10.1016/j.molliq.2019.112206.

[22] B. Sun, Y. Guo, D. Yang, H. Li, The effect of constant magnetic field on convective heat transfer of Fe3O4/water magnetic nanofluid in horizontal circular tubes, Appl. Therm. Eng. 171 (2020), https://doi.org/10.1016/j.applthermaleng.2020.114920.

[23] M. Goharkhah, A. Salarian, M. Ashjaee, M. Shahabadi, Convective heat transfer characteristics of magnetite nanofluid under the influence of constant and alternating magnetic field, Powder Technol. 274 (2015) 258–267, https://doi.org/10.1016/j.powtec.2015.01.031.

[24] M. Tekir, E. Taskesen, B. Aksu, E. Gedik, K. Arslan, Comparison of bi-directional multi-wave alternating magnetic field effect on ferromagnetic nanofluid flow in a circular pipe under laminar flow conditions, Appl. Therm. Eng. 179 (2020), https://doi.org/10.1016/j.applthermaleng.2020.115624.

[25] S. Mei, C. Qi, T. Luo, X. Zhai, Y. Yan, Effects of magnetic field on thermo-hydraulic performance of Fe3O4-water nanofluids in a corrugated tube, Int. J. Heat Mass Transf. 128 (2019) 24–45, https://doi.org/10.1016/j.ijheatmasstransfer.2018.08.071.

[26] R. Azizian, E. Doroodchi, T. McKrell, J. Buongiorno, L.W. Hu, B. Moghtaderi, Effect of magnetic field on laminar convective heat transfer of magnetite nanofluids, Int. J. Heat Mass Transf. 68 (2014) 94–109, https://doi.org/10.1016/j.ijheatmasstransfer.2013.09.011.

[27] J. Wang, G. Li, H. Zhu, J. Luo, B. Sundén, Experimental investigation on convective heat transfer of ferrofluids inside a pipe under various magnet orientations, Int. J. Heat Mass Transf. 132 (2019) 407–419, https://doi.org/10.1016/j.ijheatmasstransfer.2018.12.023.

[28] N. Hatami, A. Kazemnejad Banari, A. Malekzadeh, and A. R. Pouranfard, "The effect of magnetic field on nanofluids heat transfer through a uniformly heated horizontal tube," *Phys. Lett., Section A: General, Atomic and Solid State Physics*, vol. 381, no. 5. Elsevier B.V., pp. 510–515, Feb. 05, 2017. doi: 10.1016/j.physleta.2016.12.017.

[29] S. Ahangar Zonouzi *et al.*, "Experimental investigation of the flow and heat transfer of magnetic nanofluid in a vertical tube in the presence of magnetic quadrupole field," *Exp. Therm. Fluid Sci.*, vol. 91, pp. 155–165, Feb. 2018, doi: 10.1016/j.expthermflusci.2017.10.013.

[30] A. Ghofrani, M. H. Dibaei, A. Hakim Sima, and M. B. Shafii, "Experimental investigation on laminar forced convection heat transfer of ferrofluids under an alternating magnetic field," Exp. Therm. Fluid Sci., 49 (2013) 193–200. doi: 10.1016/j.expthermflusci.2013.04.018.

[31] M. Lajvardi, et al., Experimental investigation for enhanced ferrofluid heat transfer under magnetic field effect, J. Magn. Magn. Mater. 322 (21) (2010) 3508–3513, https://doi.org/10.1016/j.jmmm.2010.06.054.

[32] D. Guzei, A. Minakov, M. Pryazhnikov, and K. Meshkov, "Investigating the forced convection of magnetic nanofluids.".

[33] M. S. Y. Ebaid, A. M. Ghrair, M. Al-busoul, "Investigation of heat transfer enhancement using ferro-nanofluids (Fe3O4/water) in a heated pipe under the application of magnetic field," Adv. Mech. Eng., 14(6) (2022), doi: 10.1177/16878132221102647.

[34] S.O. Giwa, M. Sharifpur, J.P. Meyer, Experimental study of thermo-convection performance of hybrid nanofluids of Al2O3-MWCNT/water in a differentially heated square cavity, Int. J. Heat Mass Transf. 148 (2020), https://doi.org/10.1016/j.ijheatmasstransfer.2019.119072.

[35] S. O. Giwa, M. Sharifpur, M. H. Ahmadi, S. M. Sohel Murshed, J. P. Meyer, "Experimental investigation on stability, viscosity, and electrical conductivity of water-based hybrid nanofluid of mwcnt-fe2o3," Nanomaterials, 11(1) (2021) 1–19, doi: 10.3390/nano11010136.

[36] S. Osman, M. Sharifpur, J.P. Meyer, Experimental investigation of convection heat transfer in the transition flow regime of aluminium oxide-water nanofluids in a rectangular channel, Int. J. Heat Mass Transf. 133 (2019) 895–902, https://doi.org/10.1016/j.ijheatmasstransfer.2018.12.169.

[37] S. Suseel Jai Krishnan, M. Momin, C. Nwaokocha, M. Sharifpur, and J. P. Meyer, "An empirical study on the persuasive particle size effects over the multi-physical properties of monophase MWCNT-Al2O3 hybridized nanofluids," J. Mol. Liq., 361 (2022), doi: 10.1016/j.molliq.2022.119668.

[38] A. Arifutzzaman, A. F. Ismail, I. I. Yaacob, M. Z. Alam, and A. A. Khan, "Stability investigation of water based exfoliated graphene nanofluids," in: *IOP Conference Series: Materials Science and Engineering*, Institute of Physics Publishing, Mar. 2019. doi: 10.1088/1757-899X/488/1/012002.

[39] S.S. Jyothirmayee, P. Baskar, T. Theres, K. Sabareesh, S. Das, S. Ramaprabhu, Investigation of structural stability, dispersion, viscosity, and conductive heat transfer properties of functionalized carbon nanotube based nanofluids, J. Phys. Chem. C 115 (2011) 16737–16744, https://doi.org/10.1021/jp201672p.

[40] M. Zadkhast, D. Toghraie, A. Karimipour, Developing a new correlation to estimate the thermal conductivity of MWCNT-CuO/water hybrid nanofluid via an experimental investigation, J. Therm. Anal. Calorim. 129 (2) (2017) 859–867, https://doi.org/10.1007/S10973-017-6213-8.

[41] A. Oraon, et al., Impact of magnetic field on the thermal properties of chemically synthesized Sm-Co nanoparticles based silicone oil nanofluid, J. Therm. Anal. Calorim. 147 (3) (2022) 1933–1943, https://doi.org/10.1007/s10973-021-10572-1.

[42] B.C. Pak, Y.I. Cho, Hydrodynamic and heat transfer study of dispersed fluids with submicron metallic oxide particles, Exp. Heat Transf. 11 (2) (1998) 151–170, https://doi.org/10.1080/08916159808946559.

[43] L.S. Sundar, M.K. Singh, A.C.M. Sousa, Thermal conductivity of ethylene glycol and water mixture based Fe3O4 nanofluid, Int. Commun. Heat Mass Transf. 49 (2013) 17–24, https://doi.org/10.1016/j.icheatmasstransfer.2013.08.026.

[44] V. Chinnasamy, J. Ham, H. Cho, Comparative investigation of convective heat transfer and pressure drop characteristics of MWCNT, Fe3O4, and MWCNT/Fe3O4 nanofluids, Case Stud. Therm. Eng. 47 (2023), https://doi.org/10.1016/j.csite.2023.103095.

[45] I.U. Ibrahim, M. Sharifpur, J.P. Meyer, Experimental investigations of particle sizes effects on exergy and entropy characteristics of AL2O3 - MWCNT hybrid nanofluid along the transitional flow regime, Case Stud. Therm. Eng. 51 (2023) 103575, https://doi.org/10.1016/j.csite.2023.103575.

[46] E. Sadeghinezhad et al., "Experimental study on heat transfer augmentation of graphene based ferrofluids in presence of magnetic field", doi: 10.1016/j.applthermaleng.2016.11.199.

[47] A.J. Ghajar, L.M. Tam, Heat transfer measurements and correlations in the transition region for a circular tube with three different inlet configurations, Exp. Therm. Fluid Sci. 8 (1) (1994) 79–90, https://doi.org/10.1016/0894-1777(94)90075-2.

[48] J.A. Olivier, J.P. Meyer, Single-phase heat transfer and pressure drop of the cooling of water inside smooth tubes for transitional flow with different inlet geometries (rp-1280), HVAC R Res. 16 (4) (2010) 471–496, https://doi.org/10.1080/10789669.2010.10390916.

[49] P. F. Dunn, "Measurement and Data Analysis for Engineering and Science Second Edition , Taylor and Francis / CRC Press , c 2010 ISBN : 9781439825686," no. August 2009, pp. 1–7, 2010.

[50] M. Ashjaee, M. Goharkhah, L.A. Khadem, R. Ahmadi, Effect of magnetic field on the forced convection heat transfer and pressure drop of a magnetic nanofluid in a miniature heat sink, Heat Mass Transf. Und Stoffuebertragung 51 (7) (2015) 953–964, https://doi.org/10.1007/s00231-014-1467-1.

[51] M. Goharkhah, M. Ashjaee, M. Shahabadi, Experimental investigation on convective heat transfer and hydrodynamic characteristics of magnetite nanofluid under the influence of an alternating magnetic field, Int. J. Therm. Sci. 99 (2016) 113–124, https://doi.org/10.1016/j.ijthermalsci.2015.08.008.

[52] A. Lee, Y. Jeon, V. Chinnasamy, H. Cho, Investigation of forced convective heat transfer with magnetic field effect on water/ethylene glycol-cobalt zinc ferrite

nanofluid, Int. Commun. Heat Mass Transf. 128 (October) (2021) 105647, https://doi.org/10.1016/j.icheatmasstransfer.2021.105647.
[53] A. Shahsavar, M. Saghafian, M.R. Salimpour, M.B. Shafii, Experimental investigation on laminar forced convective heat transfer of ferrofluid loaded with carbon nanotubes under constant and alternating magnetic fields, Exp. Therm. Fluid Sci. 76 (2016) 1–11, https://doi.org/10.1016/j.expthermflusci.2016.03.010.
[54] A. Lee, C. Veerakumar, and H. Cho, "Effect of magnetic field on the forced convective heat transfer of water–ethylene glycol-based fe3 o4 and fe3 o4 –mwcnt nanofluids," *Appl. Sci.*, 11(10) (2021), doi: 10.3390/app11104683.
[55] M. Tekir, E. Taskesen, E. Gedik, K. Arslan, B. Aksu, Effect of constant magnetic field on Fe3O4-Cu/water hybrid nanofluid flow in a circular pipe, Heat Mass Transf. Und Stoffuebertragung 58 (5) (May 2022) 707–717, https://doi.org/10.1007/s00231-021-03125-7.